# Lysosomal Proteome and Secretome Analysis Identifies Missorted Enzymes and Their Nondegraded Substrates in Mucolipidosis III Mouse Cells*[S]

Giorgia Di Lorenzo‡, Renata Voltolini Velho‡, Dominic Winter§, Melanie Thelen§, Shiva Ahmadi§, Michaela Schweizer¶, Raffaella De Pace‡¶¶, Kerstin Cornils‖, Timur Alexander Yorgan**, Saskia Grüb‡, Irm Hermans-Borgmeyer¶, Thorsten Schinke**, Sven Müller-Loennies‡‡, Thomas Braulke‡§§, and Sandra Pohl‡§§

**Targeting of soluble lysosomal enzymes requires mannose 6-phosphate (M6P) signals whose formation is initiated by the hexameric N-acetylglucosamine (GlcNAc)-1-phosphotransferase complex ($\alpha_2\beta_2\gamma_2$). Upon proteolytic cleavage by site-1 protease, the $\alpha/\beta$-subunit precursor is catalytically activated but the functions of $\gamma$-subunits (Gnptg) in M6P modification of lysosomal enzymes are unknown. To investigate this, we analyzed the *Gnptg* expression in mouse tissues, primary cultured cells, and in *Gnptg* reporter mice *in vivo*, and found high amounts in the brain, eye, kidney, femur, vertebra and fibroblasts. Consecutively we performed comprehensive quantitative lysosomal proteome and M6P secretome analysis in fibroblasts of wild-type and *Gnptg*$^{ko}$ mice mimicking the lysosomal storage disorder mucolipidosis III. Although the cleavage of the $\alpha/\beta$-precursor was not affected by *Gnptg* deficiency, the GlcNAc-1-phosphotransferase activity was significantly reduced. We purified lysosomes and identified 29 soluble lysosomal proteins by SILAC-based mass spectrometry exhibiting differential abundance in *Gnptg*$^{ko}$ fibroblasts which was confirmed by Western blotting and enzymatic activity analysis for selected proteins. A subset of these lysosomal enzymes show also reduced M6P modifications, fail to reach lysosomes and are secreted, among them $\alpha$-L-fucosidase and arylsulfatase B. Low levels of these enzymes correlate with the accumulation of non-degraded fucose-containing glycostructures and sulfated glycosaminoglycans in *Gnptg*$^{ko}$ lysosomes. Incubation of *Gnptg*$^{ko}$ fibroblasts with arylsulfatase B partially rescued glycosaminoglycan storage. Combinatorial treatments with other here identified missorted enzymes of this degradation pathway might further correct glycosaminoglycan accumulation and will provide a useful basis to reveal mechanisms of selective, Gnptg-dependent formation of M6P residues on lysosomal proteins.** ***Molecular & Cellular Proteomics 17: 1612–1626, 2018. DOI: 10.1074/mcp.RA118.000720.***

Lysosomes are acidic organelles of eukaryotic cells degrading extracellular and intracellular macromolecules as well as damaged organelles by the sequential activities of more than 70 different soluble lysosomal enzymes such as glycosidases, proteases, lipases, phosphatases, sulfatases, nucleases, and accessory proteins. For the directed delivery to lysosomes, newly synthesized lysosomal enzymes are equipped with mannose 6-phosphate (M6P)[1] residues, which are generated by two enzymes. First, the *cis*-Golgi-resident GlcNAc-1-phosphotransferase catalyzes the transfer of GlcNAc-1-phosphate from UDP-GlcNAc to selected C6 hydroxyl groups of high-mannose type *N*-glycans on lysosomal enzymes. Second, the masking GlcNAc is removed by an $\alpha$-N-acetylglucosaminidase, also called uncovering enzyme, in the *trans*-Golgi network (TGN) exposing the M6P residues (1, 2). Subsequently, M6P-containing lysosomal enzymes bind to M6P receptors mediating their vesicular transport from the TGN, via the endosomal compartment to lysosomes (3).

GlcNAc-1-phosphotransferase is a hexameric complex consisting of two membrane-bound $\alpha$- and $\beta$-subunits and

From the ‡Section Biochemistry, Children's Hospital, University Medical Center Hamburg-Eppendorf, Hamburg, Germany; §Institute of Biochemistry and Molecular Biology, University of Bonn, Bonn, Germany; ¶Center for Molecular Neurobiology, University Medical Center Hamburg-Eppendorf, Hamburg, Germany; ‖Research Department Cell and Gene Therapy, Department of Stem Cell Transplantation, University Medical Center Hamburg-Eppendorf, Hamburg, Germany; **Department of Osteology and Biomechanics, University Medical Center Hamburg-Eppendorf, 20246 Hamburg, Germany; ‡‡Division Biophysics, Research Center Borstel, Leibniz Lung Center, 23845 Borstel, Germany

Received March 8, 2018, and in revised form, April 27, 2018
Published, MCP Papers in Press, May 17, 2018, DOI 10.1074/mcp.RA118.000720

two soluble γ-subunits ($\alpha_2\beta_2\gamma_2$) (4). The human α- and β-subunits are encoded by a single gene, *GNPTAB,* and synthesized as a common type III precursor membrane protein (5, 6), whereas the soluble γ-subunits are encoded by *GNPTG* (7). After assembly of the GlcNAc-1-phosphotransferase in the ER, the inactive enzyme complex is transported to the Golgi apparatus that requires a combinatorial cytoplasmic sorting motif of the α/β-subunit precursor proteins (8, 9). On arrival in the *cis*-Golgi apparatus, the α/β-subunit precursor is proteolytically cleaved by the site-1 protease into the individual α- and β-subunits, which is a prerequisite for catalytic GlcNAc-1-phosphotransferase activity (10). The mature α- and β-subunits exhibit catalytic activity and binding sites for lysosomal enzymes (11), whereas the function of the γ-subunits is poorly defined. It has been suggested that the γ-subunits enhance the recognition and M6P formation of distinct lysosomal enzymes by the α- and β-subunit (11, 12), whereas other studies failed to show direct interactions of the γ-subunits with lysosomal enzymes (6, 13). Recently, we identified the γ-subunit binding domain in a previously uncharacterized luminal region of the α-subunit required for maximum GlcNAc-1-phosphotransferase activity (14, 15).

The significance of these data is demonstrated by the existence of the autosomal recessive lysosomal storage disease, mucolipidosis type III gamma (MLIII), caused by mutations in the *GNPTG* gene. To date 32 different *GNPTG* mutations are known including 12 frameshift, 6 nonsense, 5 missense, 2 small deletion and 7 splicing mutations (7, 13, 16–28). Biochemically, the cells from MLIII patients have reduced amounts of M6P residues on lysosomal enzymes leading to their missorting and hypersecretion into the extracellular compartment (29, 30). At present, however, it is unknown which lysosomal enzymes reach lysosomes and might be limiting for lysosomal function. The subsequent reduction of several lysosomal enzymes in lysosomes may result in the accumulation of non-degraded material, which impairs cellular homeostasis. The first clinical symptoms of MLIII patients are joint stiffness of fingers, hips and shoulders, and have been observed between 5 and 10 years of life developing to moderate *dysostosis multiplex* with vertebral scoliosis (30–32). The skin may become thickened with time. Recently scleroderma-like symptoms were described in MLIII patients (28). Because skeletal dysplasia is the most prominent clinical complication in the MLIII disease, patients can survive into adulthood (33). In contrast, the total loss of GlcNAc-1-phosphotransferase activity caused by mutations in *GNPTAB* leads to complete failure to generate M6P residues on lysosomal enzymes and a fatal lysosomal disease, mucolipidosis II (MLII). The patients show progressive and severe *dysostosis multiplex* and cranofacial abnormalities, gingival hyperplasia, mental retardation, hepato- and cardiomegaly, immune defects and death in the first decade of life (30, 34, 35). However, in certain cell types (such as hepatocytes and leukocytes) and organs (liver, kidney and brain) in MLII patients and mice nearly normal level of selected lysosomal enzymes were observed, suggesting the existence of alternate M6P-independent targeting pathways (35–38). So far it is not clear whether tissue-specific expression of the γ-subunit or differences in the targeting efficiency of distinct lysosomal enzymes are responsible for the different clinical courses and features of MLII and MLIII patients. One study reports on similar *GNPTG* transcript level in human heart, brain, placenta, lung, liver, skeletal muscle, kidney, and pancreas based on Northern blot analysis (7) but lacks however, information on the expression in specific cell types.

In the present study, we determined the mRNA expression distribution of GlcNAc-1-phosphotransferase γ-subunits in a *Gnptg*$^{lacZ}$ reporter mouse at different ages in tissues that have previously not been reported to be affected in MLIII patients. In addition, the comparative lysosomal proteomes and M6P secretomes of fibroblasts from wild-type and *Gnptg*$^{ko}$ mice led to the identification of a subset of lysosomal enzymes whose lysosomal targeting depend on the presence of γ-subunits and fail to use alternative M6P-independent pathways to lysosomes. The accumulation of chondroitin sulfate/dermatan sulfate (CS/DS) glycosaminoglycans (GAG) in *Gnptg*$^{ko}$ fibroblasts correlated with low amounts of arylsulfatase B (Arsb), a key enzyme in the degradation of CS/DS. The CS/DS storage can be rescued for the most part by incubation of cells with recombinant arylsulfatase B that has been applied as enzyme replacement therapy for patients deficient for this enzyme (39).

## EXPERIMENTAL PROCEDURES

*Antibodies*—The following antibodies were used: goat anti-Creg1, goat anti-Ctsc, goat anti-Ctsz, and goat anti-Ctsl from R&D (Minneapolis, MN); goat anti-Ctsb from Neuromics (Edina, MN); goat anti-Ctsd, mouse anti-Ctss, rabbit anti-Gapdh, rabbit anti-Npc2, and mouse anti-Ctsk from Santa Cruz Biotechnology (Dallas, TX); rabbit anti-Gba, rabbit anti-Pla2g15, goat anti-transferrin, and mouse anti-α-tubulin from Sigma-Aldrich (St. Louis, MO); mouse anti-GM130 from BD Bioscience (BD Biosciences, Franklin Lakes, NJ); mouse anti-myc and rabbit anti-PDI from Cell Signaling Technology (Cambridge, UK); rat anti-Lamp1 1D4B from the Hybridoma Bank, University of Iowa, USA. The polyclonal rabbit anti-γ-subunit and monoclonal rat anti-α-subunit of GlcNAc-1-phosphotransferase and myc-tagged single-chain M6P antibody fragment are described previously (8, 40, 41). Polyclonal rabbit anti-Limp2, anti-Plbd2, anti-Clc7 and anti-Ppt1 antibodies were kindly provided by Dr. M. Schwake, University Bielefeld, Germany (42), Dr. T. Lübke, University Bielefeld, Germany (43), Dr. T. Jentsch, MDC, Berlin, Germany (44) and Dr. S. Hofmann, University of Texas, South Western Medical Center, Dallas, TX, respectively. Horseradish peroxidase (HRP)-coupled secondary

[1] The abbreviations used are: M6P, mannose 6-phosphate; CS/DS, chondroitin sulfate/dermatan sulfate; DTT, dithiothreitol; ER, endoplasmic reticulum; GAG, glycosaminoglycans; GlcNAc, N-acetylglucosamine; Gnptg, γ-subunit of GlcNAc-1-phosphotransferase; MEF, mouse embryonic fibroblasts; ML, mucolipidosis; PDI, protein disulfide isomerase; PSM, peptide-spectrum match; PNS, postnuclear supernatant; S1P, site-1 protease; SILAC, Stable isotope labeling by amino acids in cell culture; TGN, *trans*-Golgi network.

antibodies were from Dianova (Hamburg, Germany). Alexa Fluor® 546-coupled anti-mouse IgG and anti-rat IgG, Alexa Fluor® 488-coupled anti-rabbit IgG were from Thermo Fisher Scientific (Waltham, MA).

*Mice*—For generation of *Gnptg*$^{lacZ}$ and *Gnptg*$^{ko}$ mice, embryonic stem (ES) cells carrying the *Gnptg*$^{tm1a(KOMP)Wtsi}$ allele were obtained from the Knockout Mouse Program (KOMP, National Institute of Health, USA, #76092). The targeting vector used for electroporation of ES cells contained a floxed promotor-driven IRES lacZ neomycin cassette flanked by *FRT* sites, which was inserted into intron 3 of the murine *Gnptg* gene (Fig. 1*A*). The exons 4 to 11 are flanked by *loxP* sites. For generation of *Gnptg*$^{lacZ}$ mice, ES cells were injected into C57BL6/J blastocysts and subsequently implanted into the uterine horns of C57BL6/JxCBA foster mothers according to standard protocols. Resulting chimeric males from three clones were crossed with C57BL6/J mice to obtain heterozygous offspring, which were bred to generate homozygous *Gnptg*$^{lacZ}$ mice. For generation of *Gnptg*$^{ko}$ mice, homozygous *Gnptg*$^{lacZ}$ mice were mated first with C57BL6/J Flp deleter mice (45) to excise the lacZ-neocassette (Fig. 2*A*) resulting in the tm1c allele. The offspring were mated with C57BL6/J Cre deleter mice (46) to remove the floxed exons 4 to 11 through Cre-mediated recombination. Heterozygous *Gnptg*$^{ko}$ mice were then mated to generate homozygous *Gnptg*$^{ko}$ mice. For genotyping of mice, genomic DNA from tail biopsies were extracted using the KAPA Mouse Genotyping Hot Start Kit (VWR, Radnor, PA) and amplified by multiplex PCR using primers F1 (5′- GCT CCT GGC TTC GGT TAT CA-3′), F2 (5′-CAC TCA CTC TCA GCA CCT GG-3′) and R (5′-CCAGCAGGTCCCTCTTGTTT-3′) (Fig. 1*A* and 2*A*).

*Arsb*$^{+/m}$ mice were obtained from the Jackson Laboratory (#005598). Offspring from heterozygous matings was genotyped by sequencing of a PCR amplicon (primers 5′-GCT ATA TCA CGG GCA CTA ATC C-3′ and 5′-TAT CGA ATC CTC GGC GTG T-3′) for the presence of mutation c.379G>T in exon 2.

Mice were housed in a pathogen-free animal facility at the University Medical Center Hamburg-Eppendorf, and experimental procedures were performed according the institutional guidelines.

*LacZ Reporter Gene Expression Analysis*—Fresh tissue was quickly dissected, embedded and frozen in Tissue-Tek® O.C.T.™ (Sakura, Tokyo, Japan). Sections of 16–20 μm thickness were prepared with a Leica 9000 sliding microtome. The sections were permeabilized in PBS containing 0.1% sodium deoxycholate, 0.2% Nonidet P-40 and fixed in 1% paraformaldehyde and 0.2% glutardialdehyde for 5 to 10 min. After washing with PBS the sections were incubated overnight in PBS containing substrate solution: 0.02% Nonidet NP-40, 0.1% sodium deoxycholate, 5 mM $K_3Fe(CN)_6$, 5 mM $K_4Fe(CN)_6$, 10 mM $MgCl_2$ and 1 mg/ml of the β-galactosidase substrate 5-bromo-4-chloro-indolyl-β-D-galactopyranoside (X-gal) at room temperature. Pictures were taken with a Zeiss Axiophot (Oberkochen, Germany) equipped with a digital camera and software from Kappa Optronics.

*Generation of cDNA Constructs*—The constructs for C-terminally myc-tagged full-length α/β-subunit precursor (α/β-myc) of the GlcNAc-1-phosphotransferase using the expression vector pcDNA3.1D-TOPO® was previously described (9). For generation of the lentiviral α/β-myc expression vector, the α/β-myc cDNA was amplified from a pcDNA3.1D-TOPO® plasmid using the primers 5′-GAT TGG ATC CGC CAC CAT GCT GTT CAA GCT CC-3′ and 5′-CGA GTG TAC ACT ACA GAT CCT CTT CTG AGA TGA G-3′ to introduce restriction sites for BamHI and *Bsr*GI. The resulting PCR product was cloned into the LeGO-iG2 vector (47) after excision of the IRES-GFP fragment and the plasmid DNA was commercially sequenced (Seqlab, Göttingen, Germany).

*Cell Culture*—Isolation and cultivation of MEF from *Gnptg*$^{ko}$ mice were performed as described (38). For lentivirus production and transduction, VSV-G pseudotyped lentiviral particles were produced and titered as described (47). For overexpression of the myc-tagged α/β-subunit precursor, VSV-G pseudotyped lentiviral particles were produced (47) and subsequently used for transduction of MEF. To determine the number of myc-tagged α/β-subunit precursor-positive cells, MEF were permeabilized (Cytofix/Cytoperm Kit, Becton Dickinson, Franklin Lakes, NJ) and stained for the myc-tag with a custom-labeled (Pacific Blue Antibody Labeling Kit, Thermo Fisher Scientific) anti-myc antibody. Immortalization of primary MEF from *Acp2*/*Acp5*$^{-/-}$ mice (48) was conducted by lentiviral transduction as previously described (38). Transient cDNA transfection was performed using JetPEI® (VWR, Radnor, PA) according to the manufacturer′s instructions.

For macrophage and osteoclast differentiation, bone marrow was flushed out of the femora from 12 weeks old wild-type mice with α-MEM (minimal essential medium) containing 10% fetal bovine serum (α-MEM/FBS). Cells were then plated at a density of $5 \times 10^6$ cells per ml, and after 24 h the adherent cells were cultured in α-MEM/FBS containing 10 nM 1,25-dihydroxyvitamin-D3 (Sigma-Aldrich). Beginning at day 4 after seeding M-Csf and Rankl (both from Peprotech, Hamburg, Germany) were added to a final concentration of 20 ng/ml and 40 ng/ml, respectively, and cultured for 7 days to generate osteoclasts. Primary macrophages were generated by the same method without addition of Rankl. For osteoblast differentiation the bone marrow cells were cultured for 10 days in α-MEM/FBS containing 25 μg/ml ascorbic acid and 5 mM β-glycerophosphate.

Chondrocyte progenitor cells were isolated from a single sternum of 12 days old wild-type mice. Cells were separated by digesting the tissue initially in 0.1% collagenase solution followed by 0.2% collagenase solution and cultured in DMEM/Ham's F-12 (1:1)/10% FCS (Biochrome, Berlin, Germany). At a total cell confluence of 80%, chondrocyte differentiation was induced by the addition of ascorbic acid (50 μg/ml) and cultured for 10 days.

*Glycosaminoglycan Analysis*—After 4 days in culture, MEF were incubated for 24 h with serum-free Opti-MEM™ medium containing 100 μCi/ml $Na^{35}SO_4$ (Hartmann Analytic, Göttingen, Germany). Cells were then washed twice with PBS and incubated for 24 h with serum-free Opti-MEM™ medium in the presence or absence of 10 μg/ml human recombinant ARSB kindly provided by Dr. M. Vellard (Biomarin, Novato, CA). GAGs were isolated from cell lysates using DEAE-Sepharose (Sigma-Aldrich) anion exchange chromatography and subjected to digestion with heparinase I, II and III kindly provided by Dr. J. Esko, University of California, San Diego, CA (49) or chondroitinase ABC (Sigma-Aldrich). The treatment-resistant chondroitin/dermatan sulfates (CS/DS) and heparan sulfates (HS) were purified and radioactivity quantified by liquid scintillation counting (50).

*RNA Analysis*—RNAs were isolated from various tissues of 12 weeks old wild-type mice using the Nucleospin RNA II kit (Macherey-Nagel) and 1 μg of total RNA was reversed transcribed using the Verso cDNA kit (Thermo Fisher Scientific) according to the manufacturer's instructions. RNA isolation from cultured cells, cDNA synthesis and quantitative real-time PCR using pre-designed Taqman-Assays (Thermo Fisher Scientific, supplemental Table S1) were performed as previously described (10). The relative mRNA expression levels of analyzed genes were normalized to the level of *Actb* or *Gapdh* mRNA in the same cDNA using the comparative CT method ($2^{-\Delta\Delta CT}$).

*Western Blot Analysis*—After 24 h culture in serum-free Opti-MEM™ medium, cells and media were harvested. Media were concentrated 4-fold using Amicon Ultra-0.5 ml centrifugal filters (3 kDa molecular weight cut-off) (Merck, Darmstadt, Germany). Cells were lysed in PBS containing 0.5% Triton X-100 and protease inhibitors for 30 min at 4 °C. After centrifugation at 16,000 g supernatants were used for measurement of the protein content by the Roti®quant Protein Assay (Roth, Karlsruhe, Germany). For lysosomal enriched

fractions, cell pellets were resuspended in 20 mM Hepes (pH 7.4) containing 250 mM sucrose and protease inhibitors and incubated for 10 min on ice. Cells were disrupted by 30 times passage through a 24-gauge needle. Nuclei and unbroken cells were removed by centrifugation for 2 min at 1000 × *g* and 4 °C. Supernatants were further centrifuged for 20 min at 20,000 × *g* and 4 °C. Pellets representing the lysosome-enriched fraction were resuspended in PBS containing 0.5% Triton X-100 and protease inhibitors and incubated for 30 min on ice. After centrifugation for 10 min at 16,000 × *g* and 4 °C the supernatant was removed and further processed. To analyze serum, samples (50 μl) were diluted in 500 μl 20 mM Tris (pH 7.4) containing 0.5 M NaCl and protease inhibitors and incubated with 50 μl Concanavalin A-Sepharose (GE Healthcare, Buckinghamshire, UK) overnight at 4 °C. Bound material as well as cell extracts (100 μg protein), lysosome-enriched fractions (75 μg protein) and concentrated, conditioned media (100 μl) were solubilized in reducing SDS sample buffer for 5 min at 95 °C, separated by SDS-PAGE and transferred onto nitrocellulose membranes. Membranes were blocked in Tris-buffered saline (TBS, pH 7.4) containing 0.1% Tween-20 and 5% milk powder or 1% BSA for 1 h and then incubated with the respective primary antibody in the blocking buffer for 1 h or overnight at 4 °C. Blots were washed with TBS containing 0.1% Tween-20 and incubated for 1 h at room temperature with the appropriate HRP-conjugated secondary antibody diluted in blocking buffer. Membranes were washed and immunoreactive protein bands were visualized by chemiluminescence. The content of M6P-containing proteins in cell extracts and lysosomal-enriched fractions were analyzed by Western blotting using a single chain antibody fragment scFv M6P-1 as described (41).

*Enzyme Activity Measurements*—The enzymatic activities of lysosomal enzymes in the serum of mice and in protein extracts of MEF and media of cultured cells were assayed using corresponding 4-nitrophenol or 4-methylumbelliferone substrates (51). To measure Arsb activity, 5 mM 4-nitrocatechol-sulfate (Sigma-Aldrich) was used as a substrate in 100 mM Na-citrate (pH 5.5), 0.1% Triton X-100, 0.2% bovine serum albumin and 5% NaCl. The incubation was stopped by addition of 0.4 M glycine/NaOH buffer (pH 10.4) after 17 h and the liberated 4-nitrocatechol was measured at 515 nm. Measurements of GlcNAc-1-phosphotransferase activity in cell extracts of MEF was performed as described recently (52).

*Experimental Design and Statistical Rationale*—For both the the analysis of lysosomes enriched by magnetic beads and for M6P-containing proteins enriched by M6P affinity beads, three biological replicates comparing wild-type (control) and *Gnptg*$^{ko}$ MEF were performed. This number of samples was sufficient to perform the required tests for determining statistical significance of the results. For both experiments, samples were acquired as one technical replicate whereas the in-gel digested samples were divided in 10 fractions.

*Stable Isotope Labeling by Amino Acids in Cell Culture (SILAC) and Isolation of Lysosomes with Magnetic Beads*—All SILAC reagents were obtained from Thermo Fisher Scientific and Eurisotop (Saarbrücken, Germany). For lysosomal proteome analysis, MEF were cultivated for six passages in SILAC-DMEM supplemented with 10% dialyzed FBS containing either 87.8 mg/ml l-arginine HCl, 181.2 mg/ml l-lysine for light labeling of *Gnptg*$^{ko}$ cells or l-arginine-$^{13}C_6{}^{15}N_4$ and l-lysine-$^{13}C_6{}^{15}N_2$ for heavy labeling of wild-type cells. The isolation of lysosomal fractions with magnetic beads was performed as described recently (38, 53). For M6P proteome analysis, *Gnptg*$^{ko}$ and wild-type MEF were cultured for 24 h in light or heavy SILAC-DMEM supplemented with 10 mM $NH_4Cl$. Collected media were concentrated ~50-fold using Amicon Ultra-0.5 ml centrifugal filters (3 kDa molecular weight cut-off, Merck), mixed and the protein concentration determined. Aliquots corresponding to 250 μg of protein were adjusted to 500 μl using PBS containing 0.2% Triton X-100 and protease inhibitors and incubated with 30 μl scFv M6P-1 antibody immobilized to AminoLink Plus Gel beads (1 mg/ml, Thermo Fisher Scientific) at 4 °C for 4 h on a rotating wheel. After centrifugation at 1700 g for 1 min, the supernatant was removed and the beads were washed three times with PBS containing 0.2% Triton X-100 and three times with PBS.

*Sample Preparation for Mass Spectrometry*—For lysosomal proteome analysis, lysosomal eluates were processed for mass spectrometry analysis using in gel digestion as described previously (38). For M6P proteome analysis, M6P beads with bound proteins were resuspended in 50 μl 0.1 M $NH_4HCO_3$, reduced with 5 mM dithiothreitol (DTT) for 45 min at 56 °C and alkylated with 20 mM acrylamide for 30 min at room temperature. The alkylation step was quenched by addition of 5 mM DTT followed by incubation for 45 min at room temperature. After addition of 5 μg trypsin, the volume was adjusted to 100 μl using 0.1 M $NH_4HCO_3$. Samples were incubated overnight at 37 °C and 800 rpm using a Thermomixer (Eppendorf, Hamburg, Germany). The next day, beads were pelleted by centrifugation, the supernatant transferred to a new tube and the beads extracted twice at room temperature for 15 min at 800 rpm using 300 μl 5% acetonitrile (ACN), 0.1% formic acid (FA). Supernatants were pooled and the sample reduced in volume using a vacuum centrifgure at 60 °C to ~100 μl. All samples were desalted using STAGE tips (54), dried using a vacuum centrifuge and resuspended in 20 μl 5% ACN, 5% FA.

For mass spectrometric measurements, spray tips were produced in house with a P2000 laser puller (Sutter Instrument, Novato, CA) from 360 μm OD, 100 μm ID fused silica capillaries. Spray tips were packed with 5 μm particles (Reprosil C18 AQ, Dr. Maisch, Ammerbuch-Entringen, Germany) and used as analytical columns. 5 μl of sample were loaded directly onto the analytical column using 1 μl/min 100% A (water with 5% DMSO, 0.1% FA) (55) using an EASY-nLC 1000 liquid chromatography system (Thermo Fisher Scientific). Subsequently, the column was washed for 10 min with 100% A at a flow rate of 1 μl/min and peptides eluted with a linear gradient from 100% A to 65% A/35% B (ACN with 5% DMSO, 0.1% FA) in 60 or 180 min. Peptides eluting from the column were ionized in the positive ion mode using a capillary voltage of 1600 V and analyzed using an Orbitrap Velos mass spectrometer (Thermo Fisher Scientific). One survey scan was acquired at a mass range of *m/z* 400 to *m/z* 1200 and a resultion of 60000 in the Orbitrap mass analyzer, followed by fragmentation of the 10 most abundand ions in the ion trap part of the instrument. The repeat count was set to one and the dynamic exclusion window to 60 s.

*Data Analysis*—The raw files obtained from the anaylsis of lysosomal fractions were processed with Proteome Discoverer (Thermo Fisher Scientific, Version 2.0.0.802) in combination with Mascot Version 2.4. (www.matrixscience.com) against Swissprot (release date 2015_11, 549832 entries, taxonomy: Mus musculus). Propionamide was set as fixed modification at cysteine, and N-acetylation at protein N termini, oxidation at methionine, as well as stable isotope labeling at arginine (13 C (6) 15 N (4)) and lysine (13 C (6) 15 N (2)) as variable modifications. Trypsin was selected as protease and up to one missed cleavage was accepted. The search was performed with a mass tolerance of 10 ppm for precursor ions and 0.6 Da for fragment ions. Search results were processed with Proteome Discoverer, the false discovery rate (FDR) calculated by Percolator and peptide identifications accepted with a cut-off of 0.01. Data were filtered for peptide-spectrum matches (PSMs) assigned to only one accession number and the median intensity computed across all PSMs identified for the respective protein. Protein intensities of all replicates were then combined into a feature table and such identified in only one replicate were excluded. The data were log2 transformed and median normalized to reduce variance. This allowed to perform statistical

testing of differentially expressed features with the null-hypothesis assumption that all proteins are equally distributed/expressed in the data (median normalization: per sample subtraction of median intensity of all proteins intensities). Statistical analysis of the heavy to light ratios on the protein level was performed with the R package limma (56) whose applicability on mass spectrometry data is described in (57). Corrected p values were computed with the R package q value (58) for false discovery rate estimation, using the p values obtained from the rank product output. All data processing steps were implemented in Perl and R scripts.

For M6P bead derived samples, raw files were processed using Maxquant 1.5.2.8 (59) and standard settings. Propionamide at cysteine was set as fixed modification and acetylation at protein N termini as well as methionine oxidation as variable modifications. Trypsin/P was selected as protease and one missed cleavage site accepted. The precursor ion mass tolerance for the first search was set to 20 ppm and the fragment ion tolerance to 0.5 Da. Quantification was performed with SILAC 2plex using arginine $^{13}C_6{}^{15}N_4$ and lysine $^{13}C_6{}^{15}N_2$ as heavy amino acids. Samples were searched against SwissProt/TREMBL (79899 entries, release date: 09/2016) and peptides exportet at 1% FDR. For selected proteins, manual re-quantification of the Maxquant results was performed using the spectrum viewer from Xcalibur (Thermo Fisher Scientific). Extracted ion traces (XICs) of the monoisotopic precursor ions were generated and the area under the curve quantified using Xcalibur. Determined vales were further analyzed using MS Excel.

*Others*—Deglycosylation of proteins in cell extracts with peptide-N-glycosidase F and immunofluorescence microscopy of MEF were performed as described elsewhere (40). The accumulation of L-fucose-containing material has been assessed using biotinylated *Aleuria aurantia* lectin (Vector laboratories, Burlingame, CA) as described previously (51).

*Statistical Analysis*—Data represent the mean ± standard deviation (S.D.) and significance was evaluated with the unpaired, two-tailed Student *t* test (Microsoft Excel®). A result was considered statistical significant if the *p* value was ≤ 0.05 (*), ≤ 0.01 (**), ≤ 0.001 (***). For MS data of the lysosomal proteome, statistical analysis was performed as described previously (38).

## RESULTS

*Ubiquitous Expression of GlcNAc-1-phosphotransferase*—Information regarding the tissue distribution of γ-subunits is limited. The lack of suitable high-affinity antibodies hampers the detection of γ-subunit proteins in both human and murine tissues. To study the *Gnptg* expression in mice we have determined first *Gnptg* mRNA levels in 23 different tissues of 12 weeks old wild-type mice by quantitative real-time PCR. As control the *Gnptab* transcripts have been quantified. Setting *Gnptg* and *Gnptab* transcript levels in bone marrow arbitrarily to 1, the relative *Gnptg* transcript levels varied between 0.7 (heart), 4.6 (spinal cord) to 17.7 (lung) (Fig. 1*A*). Although both genes were ubiquitously expressed in all analyzed tissues, the relative transcript level of *Gnptg* was found to be constantly higher than *Gnptab*. The *Gnptg*/*Gnptab* ratio was highest in the brain, eye, liver, kidney, and thyroid gland (Fig. 1*A*). In cultured primary cells of wild-type mice characterized by the expression of specific marker genes (supplemental Fig. S1*A*), the relative transcript levels of *Gnptg* and *Gnptab* were similar except for primary osteoclasts, where the *Gnptab* mRNA expression was significantly higher than *Gnptg* (Fig. 1*B*). To analyze the *in vivo* expression of *Gnptg,* we used a *Gnptg*$^{lacZ}$ reporter mouse allowing *Gnptg* promotor-driven expression of the bacterial β-galactosidase encoded by *lacZ* (Fig. 1*C*). X-gal staining of P0 mice revealed specific *Gnptg* expression in dorsal root ganglia (Fig. 1*D*, a) and the central nervous system (Fig. 1*D*, b) of *Gnptg*$^{lacZ}$ mice, whereas unspecific β-galactosidase activity was detected in the gastro-intestinal tract of both wild-type and *Gnptg*$^{lacZ}$ mice (Fig. 1*D*, c). In P3 mice strong *Gnptg* expression was detectable in different brain regions (Fig. 1*E*, a), the olfactory epithelium (Fig. 1*E*, b), the maxilla and mandible (Fig. 1*E*, c, d), the trigeminal ganglion (Fig. 1*E*, e), and the cervical vertebra (Fig. 1*E*, f, g). In addition to the central nervous system, we also found high *Gnptg* transcript expression in the renal pelvis of the kidney, the femur, the vertebra, in the inner segments of photo receptors and ganglia cells of the retina and in the sebaceous gland of hair roots of 12 weeks old *Gnptg*$^{lacZ}$ mice (supplemental Fig. S1*B*). Our data are confirmatory with *GNPTAB* and *GNPTG* expression data in human tissues (https://gtexportal.org/home/multiGeneQueryPage). In addition, high *GNPTAB* and *GNPTG* mRNA levels were found in adrenal glands. However, these data lack information about the age, gender and number of individuals tested.

*The Lack of the γ-Subunits Results in Decreased GlcNAc-1-phosphotransferase Activity*—To generate *Gnptg*$^{ko}$ mice, we crossed *Gnptg*$^{lacZ}$ mice sequentially with mice ubiquitously expressing Flp- and Cre-recombinase, which led to the deletion of exon 4 to 11 of the *Gnptg* gene (Fig. 2*A*). Whereas the wild-type murine γ-subunit consists of 307 amino acids, the targeted deletion leads to a C-terminally truncated protein of 59 amino acids (p.S59X). The soluble γ-subunit is localized in the *cis*-Golgi apparatus but was also found to be secreted into the media of cultured cells as well as into the serum (8). Western blot analysis of serum from wild-type mice using a polyclonal antibody against the murine γ-subunit revealed an immunoreactive polypeptide of 40 kDa, which was not detectable in serum of *Gnptg*$^{ko}$ mice (Fig. 2*B*). In the serum of *Gnptab*$^{ki}$ mice, a "knock-in" mouse model for MLII (51) with C-terminally truncated, ER-localized, inactive α/β-subunit precursor of GlcNAc-1-phosphotransferase (p.G1028R*fs**16), the secreted γ-subunit was detectable in amounts comparable to wild-type mouse serum (Fig. 2*B*).

The clinical diagnosis of patients with MLIII is confirmed by (1) elevated lysosomal enzyme activities in the serum, (2) reduced GlcNAc-1-phosphotransferase activity resulting in partial loss of M6P residues, and (3) decreased activities of lysosomal enzymes in cultured fibroblasts (30). In the serum of *Gnptg*$^{ko}$ mice, the activities of the lysosomal enzymes β-hexosaminidases A/B, β-galactosidase, α-mannosidase, α-fucosidase, and arylsulfatase B were 8- to 42-fold increased compared with wild-type controls (Fig. 2*C*).

To analyze the sorting and targeting of lysosomal enzymes in more detail, we prepared MEF from wild-type and *Gnptg*$^{ko}$ mice, which were used for all further experiments. Compared

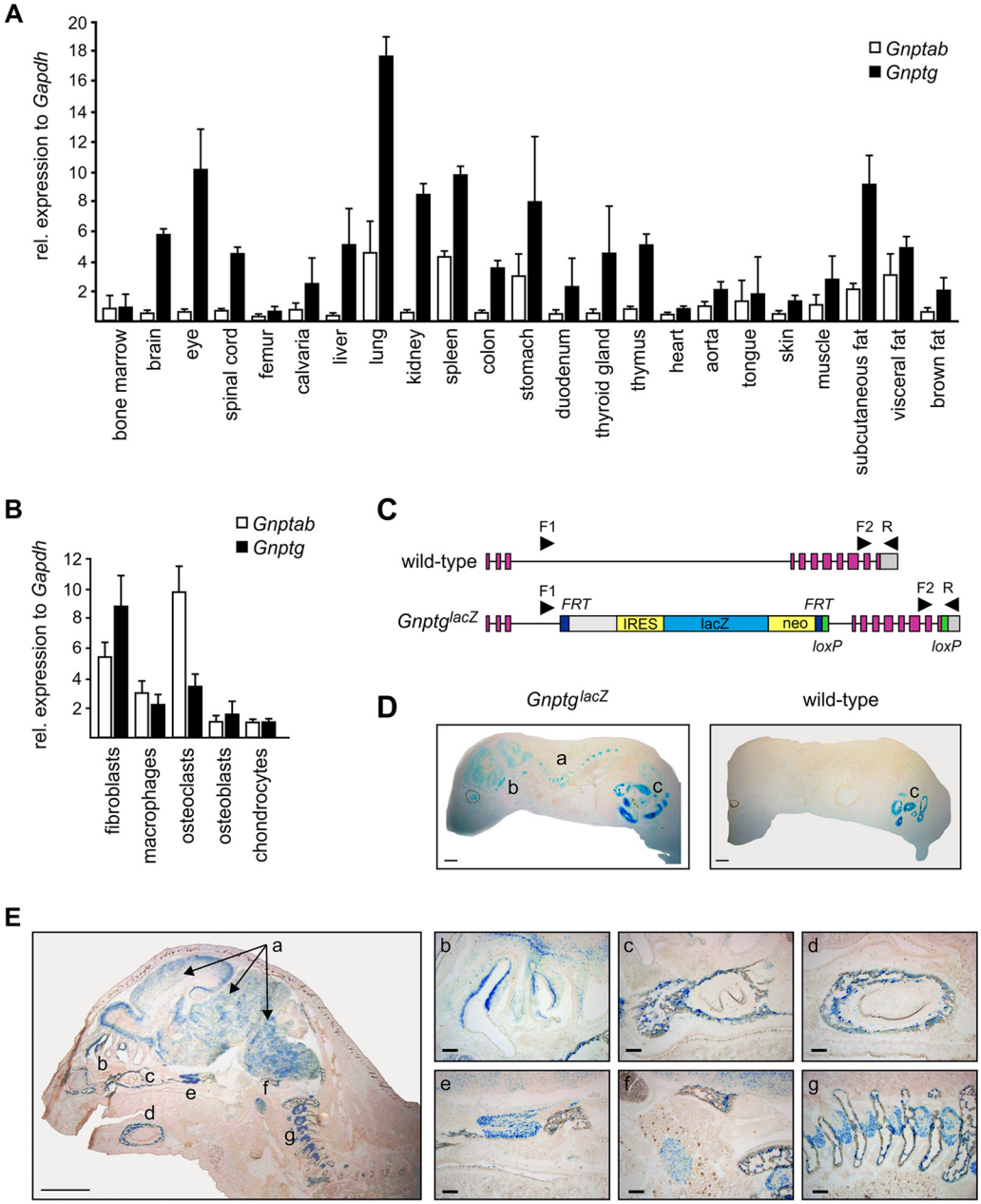


FIG. 1. ***In vivo* expression of GlcNAc-1-phosphotransferase subunits.** *A*, *Gnptab* and *Gnptg* mRNA expression in different tissues of 12 weeks old wild-type mice. The transcript level of *Gnptg* in bone marrow was assigned as 1 (mean ± S.D., $n = 4$). *B*, *Gnptab* and *Gnptg* mRNA expression in primary cultured cells of wild-type mice. The transcript level of *Gnptab* and *Gnptg* in chondrocytes was assigned as 1 (mean ± S.D., $n = 3$). *C*, Schematic presentation of murine *Gnptg* gene and $Gnptg^{lacZ}$ reporter allele. The IRES lacZ cassette with a neomycin (neo) resistance gene in the intron 3 of *Gnptg* is flanked by *FRT* (blue) and *loxP* (green) sites. Primers for genotyping of mice are indicated with arrowheads. *D,* Representative X-gal staining of P0 wild-type and $Gnptg^{lacZ}$ mice. Scale bar: 1 mm. *E*, Representative X-gal staining of different (a) brain regions, (b) olfactory epithelium, (c) maxilla and (d) mandible, (e) trigeminal ganglion, (f) first cervical vertebra (C1) and ganglia, (g) cervical vertebra and ganglia of P3 $Gnptg^{lacZ}$ mice. Scale bar left panel: 1 mm, magnified right panel b-g: 200 $\mu$m.

with wild-type, the *Gnptg* mRNA expression in $Gnptg^{ko}$ MEF was strongly reduced to 4% (Fig. 2*D*), that was confirmed by the loss of immunoreactive $\gamma$-subunits in $Gnptg^{ko}$ MEF (Fig. 2*E*). The intracellular activities of the lysosomal enzymes arylsulfatase B, $\beta$-hexosaminidase A/B, $\beta$-galactosidase, $\beta$-mannosidase, $\beta$-fucosidase were decreased to 47–18%, whereas the activity of N-acetylgalactosamine-6-sulfatase was not affected in *Gnptgko* MEF (Fig. 2*F*). When we measured GlcNAc-1-phosphotransferase activity, the loss of $\gamma$-subunits led to a decrease to 60% compared with wild-type MEF (Fig. 2*G*). Consistently, Western blot analysis using single-chain anti-M6P antibody fragments (41) showed reduced

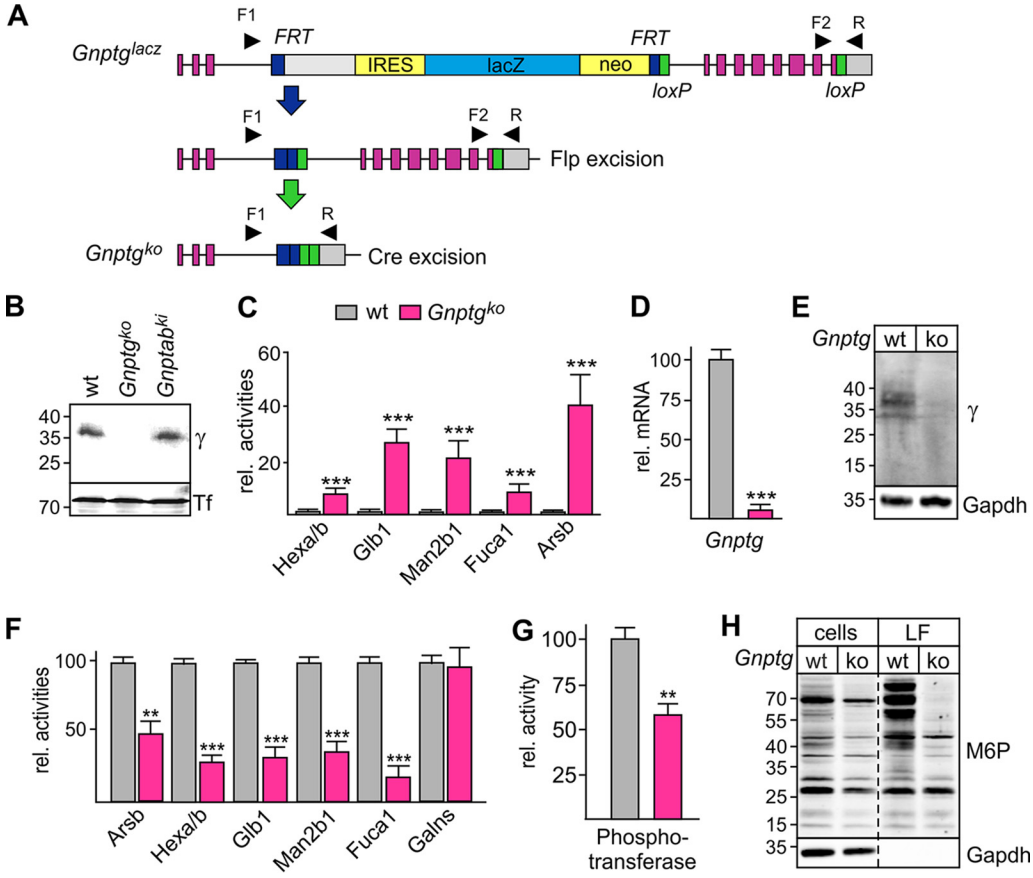


FIG. 2. **Missorting of lysosomal enzymes in *Gnptg*$^{ko}$ mice.** *A*, Schematic presentation of *Gnptg*$^{ko}$ strategy. Crossing of *Gnptg*$^{lacZ}$ mice with Flp and Cre recombinase expressing mice leads to deletion of *Gnptg* exons 4–11 in *Gnptg*$^{ko}$ mice using *FRT* and *loxP* sites, respectively (see also Fig. 1*C*). *B*, Representative Western blotting of Concanavalin A-Sepharose-enriched proteins from serum of 12 weeks old wild-type (wt), *Gnptg*$^{ko}$ and *Gnptab*$^{ki}$ mice using anti-γ-subunit antibodies. Transferrin (Tf) was used as loading control. *C*, Relative enzyme activities of β-hexosaminidase A/B (Hexa/b), β-galactosidase (Glb1), α-mannosidase (Man2b1), α-fucosidase (Fuca1) and arylsulfatase B (Arsb) in the serum of 12 weeks old wt (set as 1.0) and *Gnptg*$^{ko}$ mice (mean ± S.D., ***$p \leq 0.001$, $n = 3$). *D*, Relative mRNA expression levels of *Gnptg* in wild-type (wt, 100%) and *Gnptg*$^{ko}$ MEF (mean ± S.D., ***$p \leq 0.001$, $n = 5$). *E*, Representative γ-subunit Western blotting of cell extracts from wt and *Gnptg*$^{ko}$ MEF. Gapdh was used as loading control. *F*, Relative enzyme activities of arylsulfatase B (Arsb), β-hexosaminidases A/B (Hexa/b), β-galactosidase (Glb1), α-mannosidase (Man2b1), α-fucosidase (Fuca1) and N-acetylgalactosamine-6-sulfatase (Galns) in extracts of wt (100%) and *Gnptg*$^{ko}$ MEF (mean ± S.D., **$p \leq 0.01$, ***$p \leq 0.001$, $n = 5$). *G*, Relative GlcNAc-1-phosphotransferase activity in extracts of wt (100%) and *Gnptg*$^{ko}$ MEF (mean ± S.D., **$p \leq 0.01$, $n = 3$). *H*, M6P Western blotting of cell extracts and lysosome-enriched fractions (LF) from wt and *Gnptg*$^{ko}$ MEF. Cellular Gapdh was used as loading control.

amounts and altered pattern of M6P-containing proteins in cell extracts and lysosome-enriched fractions prepared from *Gnptg*$^{ko}$ MEF compared with wild-type controls (Fig. 2*H*).

Taken together, our data clearly show that the deficiency of γ-subunits in *Gnptg*$^{ko}$ MEF lead to decreased GlcNAc-1-phosphotransferase activity, impaired M6P formation on lysosomal enzymes and their intracellular mistargeting, the characteristic biochemical phenotype observed in patients with MLIII.

*γ-Subunit-independent Transport and Proteolytic Cleavage of the α/β-Subunit Precursor*—To exclude that decreased GlcNAc-1-phosphotransferase activity in Gnptg$^{ko}$ MEF was caused by reduced expression of the catalytically active α/β-subunit precursor, we measured the level of *Gnptab* mRNA by quantitative realtime-PCR and found no differences between wild-type and *Gnptg*$^{ko}$ MEF (Fig. 3*A*). To examine whether the γ-subunits are required for efficient ER-Golgi transport and/or proteolytic processing of the α/β-subunit precursor, *Gnptg*$^{ko}$ MEF were lentivirally transduced to express the human α/β-subunit precursor, followed by Western blotting. No immunoreactive polypeptides were detectable in cell extracts of non-transduced wild-type MEF, whereas both the 190 kDa α/β-subunit precursor and the cleaved 45 kDa β-subunit were detectable in wild-type and *Gnptg*$^{ko}$ MEF (Fig. 3*B*). In a second approach, we analyzed the localization of the α/β-subunit precursor by immunofluorescence microscopy of wild-type and *Gnptg*$^{ko}$ MEF overexpressing the α/β-subunit precursor using a monoclonal antibody against the α-subunit. Cells were co-stained for protein disulfide isomerase (PDI) or GM130 representing marker

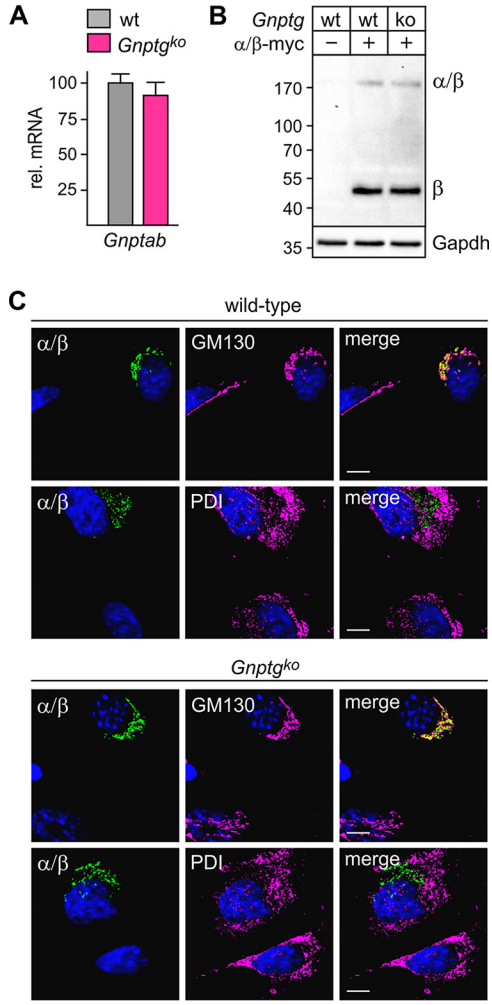


FIG. 3. **Proteolytic cleavage of the α/β-subunit precursor is independent of γ-subunits.** *A*, Relative *Gnptab* mRNA expression in wild-type (wt, 100%) and *Gnptg*$^{ko}$ MEF (mean ± S.D., $n = 3$). *B*, Representative Western blotting of cell extracts from wt and *Gnptg*$^{ko}$ MEF transduced with lentiviral particles containing human α/β-subunit precursor-myc (α/β-myc) cDNA. Gapdh was used as loading control. *C*, Immunofluorescence microscopy of wt and *Gnptg*$^{ko}$ cells transfected with human α/β-subunit precursor cDNA. Cells were stained with antibodies against the α-subunit (α/β, *green*), the marker proteins for the *cis*-Golgi apparatus (GM130, *magenta*) and the ER (PDI, *magenta*). Nuclei were visualized by DAPI (*blue*). In merged images, *yellow* indicates colocalization. Scale bars: 6 μm.

proteins for the ER and the *cis*-Golgi apparatus, respectively. In wild-type and *Gnptg*$^{ko}$ MEF α-subunit-positive signals were found exclusively in the *cis*-Golgi apparatus (Fig. 3*C*), which is confirmatory with the cleavage of the α/β-subunit precursor by S1P which is localized in the *cis*-Golgi apparatus (10, 60).

Our data show that neither mRNA expression and ER-Golgi transport nor the proteolytic cleavage of the α/β-subunit precursor depend on γ-subunits, in contrast to the maximum enzymatic activity of GlcNAc-1-phosphotransferase.

*Lysosomal Proteome of Gnptg*$^{ko}$ *Cells*—The reduced activity of GlcNAc-1-phosphotransferase in the absence of γ-subunits alters the trafficking of lysosomal enzymes to lysosomes. To determine the relative amounts of the lysosomal proteome at steady state, we performed SILAC-based comparative mass spectrometry (MS) of lysosomal fractions isolated from wild-type and *Gnptg*$^{ko}$ MEF. The cells were grown in either heavy (wild-type) or light (*Gnptg*$^{ko}$) SILAC media for six passages and then incubated with medium containing dextran-stabilized magnetites for 24 h followed by a 36 h chase period in magnetite-free heavy or light medium (Fig. 4*A*). Equal amounts of postnuclear supernatant (PNS) proteins were mixed, magnetite-containing lysosomal fractions separated on a magnetic column, and the eluate processed for MS analysis (Fig. 4*A*). We identified 103 proteins assigned to the lysosomal compartment, comprising 51 soluble proteins (Fig. 4*B*, supplemental Table S2), 40 membrane proteins (supplemental Table S3) and 12 proteins known to be associated to the lysosomal surface (supplemental Table S4). Among these proteins, only one membrane protein, *i.e.* Tpcn1 (two pore calcium channel protein 1) but 29 soluble lysosomal enzymes exhibited statistically significant reduced amounts ($p \leq 0.05$) in lysosomes of *Gnptg*$^{ko}$ cells (Fig. 4*B*). These enzymes are involved in the degradation of lipids, glycans, proteins and peptides (Fig. 4*C*).

To analyze whether mRNA expression levels contribute to altered lysosomal protein expression, we performed quantitative real-time PCR measurements from wild-type and *Gnptg*$^{ko}$ cells. Among 42 exemplary selected mRNAs of lysosomal enzymes, only the transcript level of *Ctss* was decreased by 50% in *Gnptg*$^{ko}$ compared with wild-type cells (Fig. 4*D*). The mRNA level of eight enzymes (*Manba, Aga, Dpp7, Neu1, Cln5, Epdr1, Gba,* and *Arsk*) were moderately increased whereas the *Npc2* transcript level was 2.8-fold up-regulated in *Gnptg*$^{ko}$ cells compared with controls (Fig. 4*D*). Together, the proteomic and transcriptomic data suggest that the decreased amounts of *e.g.* putative phospholipase B-like 2 (Pldb2), palmitoyl-protein thioesterase 2 (Ppt2), arylsulfatases A and B (Arsa and Arsb), phospholipase A2, group XV (Pla2g15), sialate O-acetylesterase (Siae), β-mannosidase (Manba), dipeptidyl-peptidase 7 (Dpp7), aspartylglucosaminidase (Aga) and cathepsin C (Ctsc) are caused by missorting that depends on the γ-subunit of GlcNAc-1-phosphotransferase rather than transcriptional regulation. In contrast, the amounts of 22 lysosomal enzymes were not significantly altered and therefore are transported to lysosomes with comparable efficiency as in wild-type cells (Fig. 4*B*).

To verify the proteomic data, we performed Western blot analysis of cell extracts, corresponding media and lysosome-enriched fractions for selected lysosomal enzymes. In agreement with the comparative proteomic data and mRNA expression the amounts of β-glucocerebrosidase (Gba), delivered to lysosomes in an M6P-independent manner by lysosomal integral membrane protein Limp2 (61), was increased in cell extracts and lysosomal fractions of *Gnptg*$^{ko}$ cells compared with controls (Fig. 5, left panel). Likewise, the increased *Npc2*

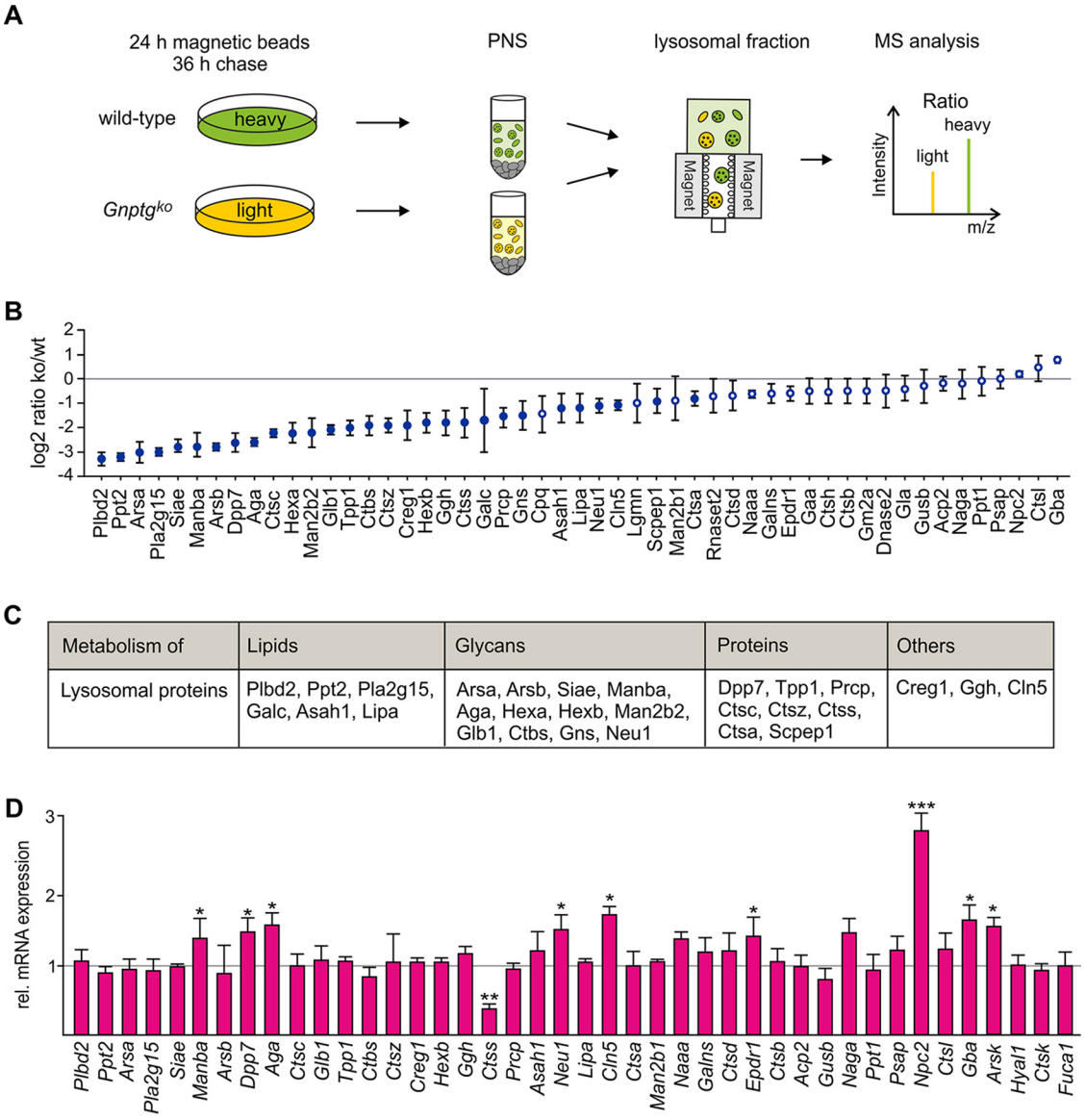


FIG. 4. **SILAC-based quantitative lysosomal proteome analysis revealed missorting of specific lysosomal enzymes in *Gnptg*$^{ko}$ MEF.** *A*, Schematic presentation of lysosomal proteome analysis. MEF were grown in light (*Gnptg*$^{ko}$) and heavy-isotope (wild-type) labeled medium, incubated with magnetite particles followed by a 36 h chase to allow magnetic beads accumulation in lysosomes. Equal amounts of postnuclear supernatants (PNS) proteins from both cell lines were combined, followed by magnetic isolation of lysosomes and MS analysis. *B*, Comparative proteomic data of soluble lysosomal proteins are displayed as Log2 ko/wt (light/heavy) ratio (mean ± S.D., $n = 3$, $p$ values are given in supplemental Table S2). Significantly reduced lysosomal enzymes in *Gnptg*$^{ko}$ samples are indicated by closed circles. *C*, Low concentrations of soluble lysosomal proteins in *Gnptg*$^{ko}$ lysosomal fractions involved in different degradation pathways: putative phospholipase B-like 2 (Pldb2), palmitoyl-protein thioesterase 2 (Ppt2), group XV phospholipase A2 (Pla2g15), galactocerebrosidase (Galc), acid ceramidase (Asah1), lysosomal acid lipase (Lipa), arylsulfatases A and B (Arsa, Arsb), sialate O-acetylesterase (Siae), β-mannosidase (Manba), aspartylglucosaminidase (Aga), β-hexosaminidase A and B (Hexa, Hexb), α-mannosidase (Man2b2), β-galactosidase (Glb1), di-N-acetylchitobiase (Ctbs), N-acetylglucosamine-6-sulfatase (Gns), sialidase 1 (Neu1), dipeptidyl-peptidase 7 (Dpp7), tripeptidyl peptidase 1 (Tpp1), prolylcarboxypeptidase (Prcp), cathepsins C, Z, S and A (Ctsc, Ctsz, Ctss, Ctsa), serine carboxypeptidase 1 (Scpep1), Creg1 protein, γ-glutamyl hydrolase (Ggh) and neuronal ceroid-lipofuscin protein 5 (Cln5). *D*, Relative mRNA expression levels of indicated genes encoding soluble lysosomal enzymes were determined in wt (1.0) and *Gnptg*$^{ko}$ MEF (mean ± S.D., $^{*}p \leq 0.05$, $^{**}p \leq 0.01$, $^{***}p \leq 0.001$, $n = 3$).

mRNA expression was also detectable on protein level in the lysosome-enriched fraction of *Gnptg*$^{ko}$ cells (Fig. 5, left panel). The amount of Ctsl and Ppt1 in lysosomal fractions of *Gnptg*$^{ko}$ cells was not altered, but notably Ppt1 was found to be more secreted into media of cultured *Gnptg*$^{ko}$ cells compared with controls (Fig. 5, left panel). Ctsk was not identified by mass spectrometry, but based on western blots we observed lysosomal delivery of Ctsk in control and *Gnptg*$^{ko}$ cells. The decreased electrophoretic mobility of precursor and mature Ctsk forms was caused by altered *N*-glycan processing in

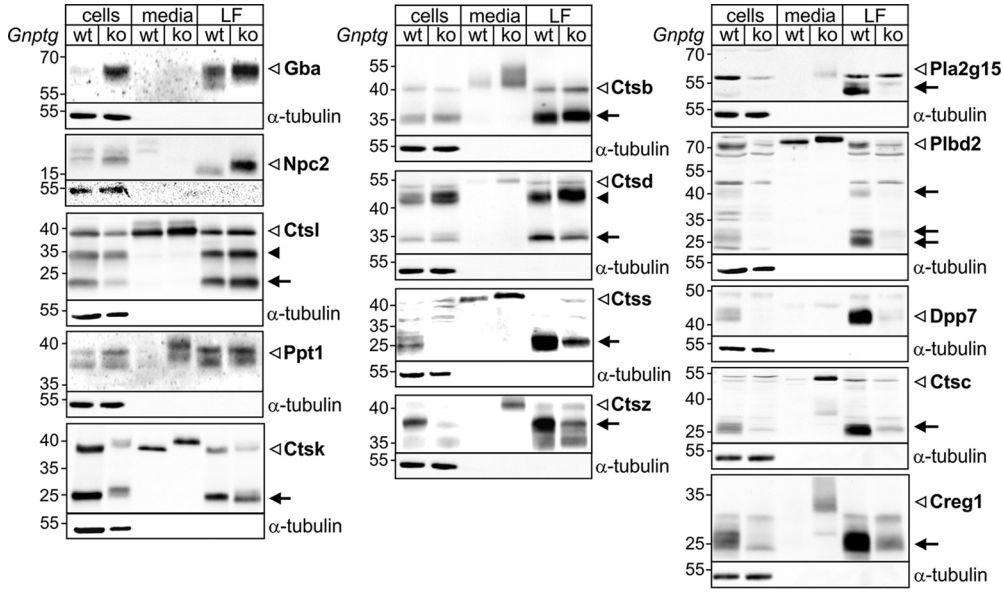


FIG. 5. **Missorting and altered lysosomal processing of specific soluble lysosomal proteins in *Gnptg*$^{ko}$ MEF.** Representative western blots of whole cell extracts (100 $\mu$g protein), aliquots (20%) of conditioned, corresponding media, and lysosome-enriched fractions (LF, 75 $\mu$g protein) from wild-type (wt) and *Gnptg*$^{ko}$ (ko) MEF using antibodies against various soluble lysosomal proteins as indicated. Endogenous $\alpha$-tubulin in cell extracts was used as loading control. The positions of precursors (non-filled arrowheads), intermediates (black arrowheads), and mature (black arrows) forms of the lysosomal enzymes are indicated.

*Gnptg*$^{ko}$ cells (supplemental Fig. S2). In addition to Ctsk, several other lysosomal proteins, such as Gba, Npc2, Ctsz, Ctsc and Creg1 differ in molecular mass and/or electrophoretic mobility in lysosome-enriched fractions of *Gnptg*$^{ko}$ cells from their corresponding wild-type forms which are most likely caused by the shift to complex oligosaccharides in the absence of M6P residues. The cathepsin proteases Ctsb, Ctsd, Ctss and Ctsz were found to be partially missorted into the media and less present in lysosome-enriched fractions of cultured *Gnptg*$^{ko}$ cells (Fig. 5, middle panel). Moreover, the steady-state level of Pla2g15, Plbd2, Dpp7, Ctsc and Creg1 were strongly reduced in lysosome-enriched fractions of *Gnptg*$^{ko}$ MEF (Fig. 5, right panel), in agreement with the data from the lysosomal proteome analysis but this appears not to be linked to hypersecretion. These data suggest that the loss of $\gamma$-subunits results in missorting and elevated secretion of some lysosomal proteins which either lead to lower abundance in lysosomes associated with alterations in peptide and glycan processing of other enzymes (*e.g.* Ctss, Ctsz, Ctsc, Creg1), or with increased instability of further subsets of soluble lysosomal proteins (*e.g.* Pla2g15, Plbd2, Dpp7).

In contrast to soluble lysosomal proteins, the mRNA and protein expression of the lysosomal membrane proteins Clc7, Limp2, and Lamp1 were only marginally altered in *Gnptg*$^{ko}$ cells. Of note, increased intensity and number of Limp2-positive structures as well as elevated concentration of Limp2 in lysosomes of *Gnptg*$^{ko}$ MEF were detected by immunofluorescence microscopy and mass spectrometry, respectively (supplemental Fig. S3 and supplemental Table S3).

*M6P Secretome of Gnptg*$^{ko}$ *Cells*—The comparative quantification of lysosomal proteins in *Gnptg*$^{ko}$ cells and the validation experiments demonstrate that the lysosomal targeting of several soluble lysosomal proteins depends on the $\gamma$-subunits of GlcNAc-1-phosphotransferase. To examine the direct role of $\gamma$-subunits for M6P generation on total soluble lysosomal proteins, we analyzed the proportion of M6P modifications of newly synthesized lysosomal proteins collected from media after $NH_4Cl$ treatment. MEF were grown for 24 h in light (*Gnptg*$^{ko}$) and heavy-isotope (wild-type) labeled medium containing 10 mM $NH_4Cl$, which increases the pH of acidic compartments, such as TGN, endosomes and lysosomes (62, 63). Under these conditions, the pH-induced dissociation of newly synthesized lysosomal enzymes from M6P receptors is prevented leading to ligand-occupied cellular M6P receptors with associated hypersecretion of newly synthesized lysosomal enzymes, and block of M6P-dependent endocytosis of extracellular lysosomal enzymes (64). Equal amounts of concentrated media from both cell lines were combined, followed by M6P affinity chromatography, trypsin digestion of bound proteins and MS analysis (Fig. 6*A*). Among 355 proteins identified, we found 33 soluble lysosomal proteins in amounts sufficient for quantification (supplemental Fig. S4 and supplemental Table S5). Among those, 11 lysosomal enzymes were significantly reduced in the bound fraction of the M6P affinity matrix of media from *Gnptg*$^{ko}$ cells, *i.e.* tripeptidyl peptidase 1 (Tpp1), putative phospholipase B-like 2 (Pldb2), prolylcarboxypeptidase (Prcp), cathepsin K (Ctsk), Creg1 protein, arylsulfatase B (Arsb), $\beta$-galactosidase (Glb1), $\beta$-hexosamini-

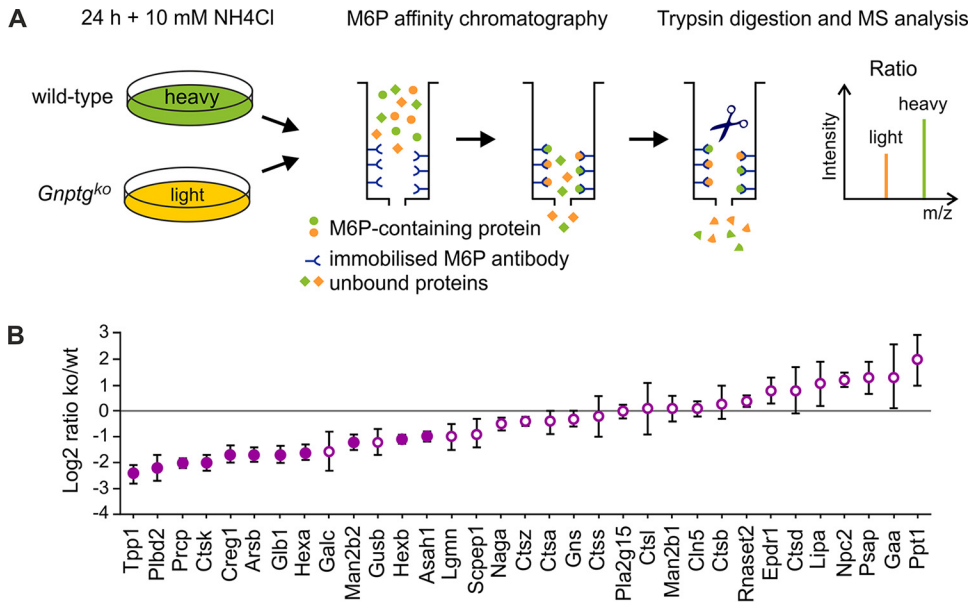


FIG. 6. **Selective M6P formation on lysosomal enzymes in *Gnptg*$^{ko}$ MEF.** *A*, Schematic presentation of M6P proteome analysis. MEF were grown in light (*Gnptg*$^{ko}$) and heavy-isotope (wild-type, wt) labeled medium containing 10 mM $NH_4Cl$. Equal amounts of concentrated media from both cell lines were combined, followed by M6P affinity chromatography, trypsin digestion of bound proteins and MS analysis. *B*, Comparative M6P proteome data of identified soluble lysosomal proteins are displayed as Log2 ko/wt (light/heavy) ratio (mean ± S.D., $n = 3$, $p$ values are given in supplemental Table S5). Significantly reduced lysosomal enzymes in *Gnptg*$^{ko}$ samples are indicated by filled circles.

dase A/B (Hexa and Hexb), α-mannosidase (Man2b2), and acid ceramidase (Asah1) (Fig. 6*B*). Although increased amounts of Ppt1, Ctsk, Ctsd, Ctsz, Plbd2, and Creg 1 have been detected in the medium of *Gnptg*$^{ko}$ cells (Fig. 5), the fraction of these proteins which bound to the M6P affinity matrix is reduced, demonstrating that these enzymes are M6P-modified to a lesser extent.

*Loss of Arylsulfatase B Causes Accumulation of Sulfated Glycosaminoglycans in Gnptg*$^{ko}$ *MEF*—Next we determined the impact of differently missorted lysosomal enzymes on lysosomal homeostasis, in particular the accumulation of partial/non-degraded storage material related to α-L-fucosidase and arylsulfatase B. The dramatic intracellular loss of α-L-fucosidase activity (Fig. 2) suggested the storage of L-fucose-containing glycostructures. Indeed, binding of the L-fucose-specific *Aleuria aurantia* lectin (AAL) was found in lysosomes in co-localization with Limp2 and at the plasma membrane of *Gnptg*$^{ko}$ cells, whereas in wild-type cells faint fucose reactivity was observed in Limp2-positive lysosomes (supplemental Fig. S5). Second, we studied the effect of low lysosomal level of arylsulfatase B (Arsb, N-acetylgalactosamine-4 sulfatase) that functions in lysosomal removal of C4 sulfate groups from chondroitin sulfate and dermatan sulfate (CS/DS) glycosaminoglycans (GAGs). At baseline the [$^{35}SO_4$] content after a 24 h pulse and 24 h chase period in MEF and total GAG fractions were 6.0- and 6.2-fold higher, respectively, in *Gnptg*$^{ko}$ compared with wild-type controls (Fig. 7*A*, 7*B*). After treatment of equal amounts of purified GAGs with chondroitinase ABC or heparin lyases I, II, and III, the resistant heparansulfate (HS) and CS/DS, respectively, were quantified and revealed to be 5.5- and 10.5-fold higher in *Gnptg*$^{ko}$ MEF (Fig. 7*C*). When we incubated the cells during the chase period in the presence of 75 nM recombinant human ARSB, the intracellular ARSB activity increased 5.2- and 5.0-fold in wild-type and in *Gnptg*$^{ko}$ MEF, respectively (Fig. 7*D*). Under these conditions the $^{35}SO_4$-labeled HS fraction from *Gnptg*$^{ko}$ cells was not affected whereas the accumulation of $^{35}SO_4$-labeled CS/DS fraction was reduced by 42% (Fig. 7*C*). The partial ARSB-mediated reduction in CS/DS level is not because of limiting amounts of endocytosed ARSB because parallel incubation of *Arsb*$^{ko}$ cells completely rescued the storage of $^{35}SO_4$-labeled CS/DS (supplemental Fig. S6). These data demonstrate that in the absence of GlcNAc-1-phosphotransferase γ-subunits the efficiency of M6P formation on Arsb is low and results in its missorting, intracellular loss and subsequent accumulation of CS/DS. Exogenous supplementations of *Gnptg*$^{ko}$ cells with recombinant ARSB led to high lysosomal ARSB activity and partial correction of the lysosomal storage material, indicating that Arsb missorting in *Gnptg*$^{ko}$ cells plays the major critical role in CS/DS degradation.

## DISCUSSION

Previous studies have shown that in the absence of the γ-subunit of GlcNAc-1-phosphotransferase the extent of M6P modification of two third of all lysosomal enzymes was decreased which correlated with a reduced GlcNAc-1-phosphotransferase activity (11, 12, 14). This implicates the reduced binding capacity of newly synthesized lysosomal enzymes to and impaired intracellular sorting mediated by M6P receptors. This is the rationale behind the determination of increased

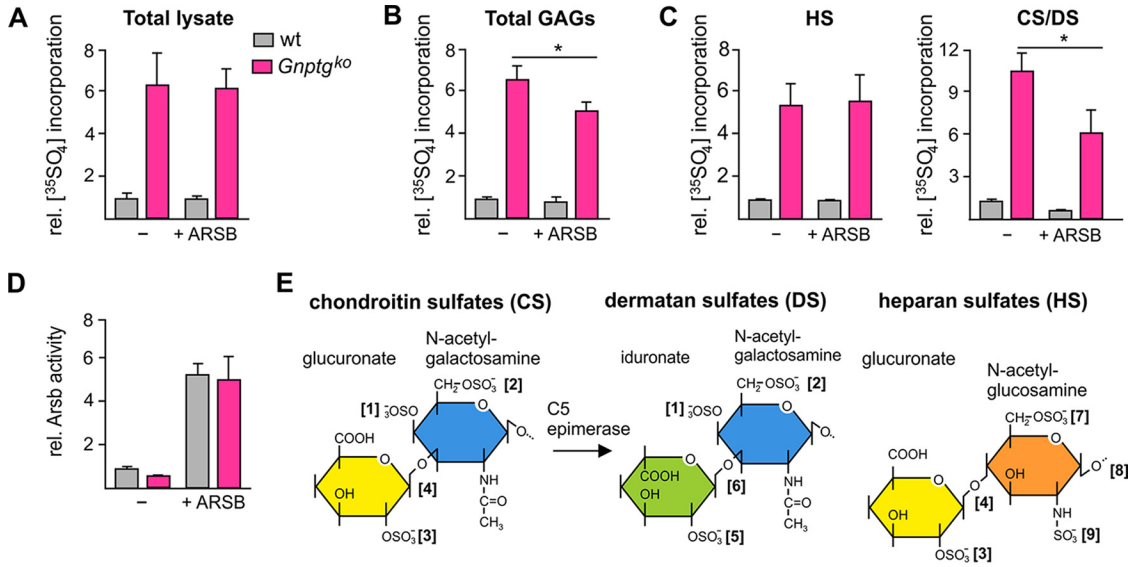


FIG. 7. **Loss of ARSB causes accumulation of sulfated GAGs in *Gnptg*$^{ko}$ MEF.** *A*, Relative [$^{35}SO_4$] incorporation in wild-type (wt) and *Gnptg*$^{ko}$ MEF after 24 h pulse and 24 h chase in the absence (−) or presence (+) of human recombinant ARSB measured in the total lysate (non-treated wt = 1; $n = 2$; wt values experiment 1: 112 cpm/$\mu$g, experiment 2: 679 cpm/$\mu$g). *B*, Quantification of purified $^{35}SO_4$-labeled GAGs (non-treated wt = 1; $^*p \leq 0.05$, $n = 2$; wt values experiment 1: 203 cpm/$\mu$g, experiment 2: 478 cpm/$\mu$g). *C*, Quantification of purified $^{35}SO_4$-labeled HS and CS/DS after digestion with chondroitinase or heparinase, respectively (non-treated wt = 1; $^*p \leq 0.05$, $n = 2$; wt values experiment 1: HS: 21 cpm/$\mu$g, CS/DS: 17 cpm/$\mu$g; experiment 2: HS: 50 cpm/$\mu$g; CS/DS: 66 cpm/$\mu$g). *C*, Relative enzyme activities of Arsb in wt and *Gnptg*$^{ko}$ MEF in the absence (−) or presence (+) of ARSB (non-treated wt = 1; mean ± S.D., $n = 2$). *D*, Overview of CS/DS and HS degradation. The numbers in brackets indicate the respective lysosomal enzymes. 1: Arsb, 2: Galns, 3: Gds, 4: Gusb, 5: Ids, 6: Idua, 7: Gns, 8: Naglu, 9: Sgsh.

lysosomal enzyme activities in the serum of patients and mice carrying mutations in the $\alpha$-, $\beta$-, or $\gamma$-subunit encoding genes as diagnostic parameters (7, 21, 51, 65).

The present study provides several new insights into the role of the $\gamma$-subunits of the hexameric GlcNAc-1-phosphotransferase complex for lysosomal functions in general, and its impact on specificity for substrate degradation. The comparative SILAC-based analyses of the lysosomal proteome and the M6P secretome of MEF derived from *Gnpg*$^{ko}$ mice allowed us to correlate the extent of M6P modification of lysosomal enzymes with M6P-dependent and -independent lysosomal targeting mechanisms.

The $\alpha/\beta$-subunit precursors and $\gamma$-subunit dimers assemble in the ER to an enzymatically inactive complex and upon arrival in the Golgi-apparatus the $\alpha/\beta$-subunit precursors are cleaved by site-1 protease (S1P) forming a catalytically active hexameric complex (8, 10). Here we could show that the $\gamma$-subunits are neither essential for the export of the $\alpha/\beta$-subunit precursor from the ER nor for S1P-mediated proteolytic cleavage in the Golgi apparatus. However, $\gamma$-subunits are important to (1) maintain maximum GlcNAc-1-phosphotransferase activity, and (2) promote the M6P modification of a subset of ~10 soluble lysosomal proteins which concentrations are therefore very low in lysosomes of *Gnptg*$^{ko}$ cells (< 20% of controls). Kornfeld and colleagues have analyzed the brain M6P proteome of *Gnptg*$^{ko}$ mice using an M6P receptor affinity chromatographic approach and found that 25% of the lysosomal enzymes were poorly modified with M6P residues (11). Although this approach does not provide information on the cellular origin or intracellular localization of M6P-containing lysosomal enzymes in the brain, nine of 12 lysosomal proteins with the lowest affinity for the M6P receptor matrix were identical with the lowest abundant proteins identified here in lysosomes of *Gnptg*$^{ko}$ MEF. These different data sets suggest that the $\gamma$-subunit-dependent M6P modification is specific and cell-independent for a subset of lysosomal proteins. However, our analyses could not confirm the effects of missing $\gamma$-subunits on the selective M6P modification of glycosidases *versus* cathepsin proteinases as reported in *Gnptg*-deficient zebrafish (66).

An interesting observation is the transcriptional up-regulation of *Npc2* in *Gnptg*$^{ko}$ MEF (Fig. 4*D*). *Npc2* encodes Niemann-Pick type C2 protein that binds non-esterified cholesterol in the lumen of lysosomes and transfers it to Npc1, facilitating the egress of cholesterol from lysosomes (67). Consequently, to the *Npc2* mRNA level, double amounts of newly synthesized M6P-modified Npc2 was found to be secreted into the medium (Fig. 6*B*) as well as increased concentrations of immunoreactive Npc2 in lysosomal fractions of *Gnptg*$^{ko}$ MEF were detected (Fig. 5). It is likely that the elevated level of M6P-containing Npc2 in brain extracts of *Gnptg*$^{ko}$ mice (11) is also caused by transcriptional activation. It has been reported that the inhibition of histon deacetylase 1/2 (HDAC1/2) by administration of specific inhibitors or sphingosine 1-phosphate enhances the expression of Npc1 and Npc2 (68–70). The signaling mecha-

nism, most likely initiated by dysfunctional lysosomes, to control the selective transcriptional regulation of *Npc2* in γ-subunit-deficient MEF, and presumably brain cells, is needed to be examined.

The analysis of the lysosomal proteome and M6P secretome also allowed for the first time a directed approach to identify storage material in *Gnptg*$^{ko}$ MEF. Thus, the intracellular absence of α-L-fucosidase in *Gnptg*$^{ko}$ cells suggests an incapability of the GlcNAc-1-phosphotransferase to modify α-L-fucosidase with M6P residues that leads to its subsequent missorting. Similarly to MEF deficient for functional α/β-subunits (38), there are no alternate transport mechanisms for nonphosphorylated α-L-fucosidase to lysosomes. In contrast this does not apply for liver cells (71). Indeed, we identified the accumulation of nondegraded fucose-containing material by fucose-specific lectin staining in lysosomes of *Gnptg*$^{ko}$ MEF (supplemental Fig. S5). Furthermore, the intracellular concentrations of enzymes involved in GAG degradation (Fig. 7*E*) such as Arsb, Glb1, Hexa/b, and Gns were found to be low in *Gnptg*$^{ko}$ MEF (Fig. 2 and 4). In addition, Arsb, Gns and Gusb were only weakly decorated with M6P residues (Fig. 6*B*). Therefore, we predicted impaired capabilities for degradation of GAGs in *Gnptg*$^{ko}$ MEF, that was demonstrated by the accumulation of $^{35}$S-labeled heparan sulfate (HS) and chondroitin/dermatan sulfate (CS/DS) proteoglycans (Fig. 7*C*). The supplementation with human recombinant ARSB led to significant reduction of CS/DS accumulation in *Gnptg*$^{ko}$ MEF (Fig. 7*C*). The failure to reduce the accumulation of CS/DS proteoglycans by ARSB supplementation completely is most likely because of the concomitant lack of other essential lysosomal glycosidases and sulfatases rather than limiting amounts of recombinant ARSB (supplemental Fig. S6). Other lysosomal enzymes available as recombinant drugs for single enzyme replacement therapy of mucopolysaccharidosis patients, which could be able to decrease GAG storage in combination with ARSB in *Gnptg*$^{ko}$ cells remain to be identified. Because skeletal dysplasia and destruction of the hip joints are the most disabling features in MLIII patients, it is essential to study whether the low expression of *Gnptg* compared with *Gnptab* in osteoclasts are related to skeletal abnormalities and similar changes in the lysosomal proteome as reported here in MEF. The combinatorial application of approved lysosomal enzymes with ARSB might represent a novel therapeutic strategy for treatment of MLIII patients.

*Acknowledgments*—We thank Johannes Brand, Emanuela Szpotowicz, Anke Jeschke, Josephine Knickrehm, Nadine Harmel, Ute Agge, and Nahal Brocke-Ahmadinejad for excellent technical assistance. The GAG analysis and fluorescence microscopic evaluation were supported by the Isotopic Lab and the Microscopy Imaging Facilities of the University Medical Center Hamburg-Eppendorf, respectively. We thank Kristoffer Riecken for providing the lentiviral LeGO-iCer2 and LeGO-iG2 vectors and Till Köhne for the help for X-Gal staining of jawbones.

DATA AVAILABILITY

The mass spectrometry proteomics datasets have been deposited to the Proteome X-change consortium with the dataset identifiers PXD007547 (lysosomal proteome analysis) and PXD009621 (M6P secretome analysis). Furthermore, M6P secretome data have been uploaded to MS-Viewer (72) with the dataset identifiers 2jfxtukaeg (60 min gradients) and ku5ioubkjq (180 min gradients).

* This work was funded by Deutsche Forschungsgemeinschaft (GRK1459, PO 1539/1-1, SFB877, FOR2625).

S This article contains supplemental material.

§§ To whom correspondence should be addressed: Section Biochemistry, Children's Hospital, University Medical Center Hamburg-Eppendorf, Martinistrasse 52, 20246 Hamburg, Germany. Tel.: +49 40 7410 58780; Fax: +49 40 7410 58504; E-mail: s.pohl@uke.de or braulke@uke.de.

¶¶ Present address: Cell Biology and Neurobiology Branch, Eunice Kennedy Shriver National Institute of Child Health and Human Development, NIH, 20847 Bethesda, MD.

Author contributions—G.D.L., R.V.V., D.W., M.T., S.A., M.S., R.D.P., K.C., T.A.Y., S.G., T.S., and S.P. performed the experiments and/or analyzed the data. I.H.B. generated *Gnptg*$^{lacZ}$ and *Gnptg*$^{ko}$ mice. S.M.L. provided scFv M6P-1 antibody immobilized to beads. T.B. and S.P. designed the study, supervised the work and wrote the manuscript.

REFERENCES

1. Pohl, S., Marschner, K., Storch, S., and Braulke, T. (2009) Glycosylation- and phosphorylation-dependent intracellular transport of lysosomal hydrolases. *Biol. Chem.* **390,** 521–527
2. Reitman, M. L., and Kornfeld, S. (1981) Lysosomal enzyme targeting. N-Acetylglucosaminylphosphotransferase selectively phosphorylates native lysosomal enzymes. *J. Biol. Chem.* **256,** 11977–11980
3. Braulke, T., and Bonifacino, J. S. (2009) Sorting of lysosomal proteins. *Biochim. Biophys. Acta* **1793,** 605–614
4. Bao, M., Booth, J. L., Elmendorf, B. J., and Canfield, W. M. (1996) Bovine UDP-N-acetylglucosamine:lysosomal-enzyme N-acetylglucosamine-1-phosphotransferase. I. Purification and subunit structure. *J. Biol. Chem.* **271,** 31437–31445
5. Kudo, M., Bao, M., D'Souza, A., Ying, F., Pan, H., Roe, B. A., and Canfield, W. M. (2005) The alpha- and beta-subunits of the human UDP-N-acetylglucosamine:lysosomal enzyme N-acetylglucosamine-1-phosphotransferase [corrected] are encoded by a single cDNA. *J. Biol. Chem.* **280,** 36141–36149
6. Tiede, S., Storch, S., Lübke, T., Henrissat, B., Bargal, R., Raas-Rothschild, A., and Braulke, T. (2005) Mucolipidosis II is caused by mutations in GNPTA encoding the alpha/beta GlcNAc-1-phosphotransferase. *Nat. Med.* **11,** 1109–1112
7. Raas-Rothschild, A., Cormier-Daire, V., Bao, M., Genin, E., Salomon, R., Brewer, K., Zeigler, M., Mandel, H., Toth, S., Roe, B., Munnich, A., and Canfield, W. M. (2000) Molecular basis of variant pseudo-hurler polydystrophy (mucolipidosis IIIC). *J. Clin. Invest.* **105,** 673–681
8. Encarnação, M., Kollmann, K., Trusch, M., Braulke, T., and Pohl, S. (2011) Post-translational modifications of the gamma-subunit affect intracellular trafficking and complex assembly of GlcNAc-1-phosphotransferase. *J. Biol. Chem.* **286,** 5311–5318
9. Franke, M., Braulke, T., and Storch, S. (2013) Transport of the GlcNAc-1-phosphotransferase alpha/beta-subunit precursor protein to the Golgi apparatus requires a combinatorial sorting motif. *J. Biol. Chem.* **288,** 1238–1249
10. Marschner, K., Kollmann, K., Schweizer, M., Braulke, T., and Pohl, S. (2011) A key enzyme in the biogenesis of lysosomes is a protease that regulates cholesterol metabolism. *Science.* **333,** 87–90
11. Qian, Y., Lee, I., Lee, W., Qian, M., Kudo, M., Canfield, W., Lobel, P., and Kornfeld, S. (2010) Functions of the alpha, beta, and gamma subunits of

UDP-GlcNAc:lysosomal enzyme N-acetylglucosamine-1-phosphotransferase. *J. Biol. Chem.* **285,** 3360–3370
12. Lee, W. S., Payne, B. J., Gelfman, C. M., Vogel, P., and Kornfeld, S. (2007) Murine UDP-GlcNAc:lysosomal enzyme N-acetylglucosamine-1-phosphotransferase lacking the gamma-subunit retains substantial activity toward acid hydrolases. *J. Biol. Chem.* **282,** 27198–27203
13. Pohl, S., Tiede, S., Castrichini, M., Cantz, M., Gieselmann, V., and Braulke, T. (2009) Compensatory expression of human N-Acetylglucosaminyl-1-phosphotransferase subunits in mucolipidosis type III gamma. *Biochim. Biophys. Acta* **1792,** 221–225
14. De Pace, R., Velho, R. V., Encarnacao, M., Marschner, K., Braulke, T., and Pohl, S. (2015) Subunit interactions of the disease-related hexameric GlcNAc-1-phosphotransferase complex. *Hum. Mol. Genet.* **24,** 6826–6835
15. Velho, R. V., De Pace, R., Tidow, H., Braulke, T., and Pohl, S. (2016) Identification of the interaction domains between alpha- and gamma-subunits of GlcNAc-1-phosphotransferase. *FEBS Lett.* **590,** 4287–4295
16. Barea, J. J., van Meel, E., Kornfeld, S., and Bird, L. M. (2015) Tuberous sclerosis, polycystic kidney disease and mucolipidosis III gamma caused by a microdeletion unmasking a recessive mutation. *Am. J. Med. Genet. A.* **167A,** 2844–2846
17. Encarnação, M., Lacerda, L., Prata, R. C. M. J., Coutinho, M. F., Ribeiro, H., Lopes, L., Pineda, M., Ignatius, J., Galvez, H., Mustonen, A., Lima, M. R., and Alves, S. (2009) Molecular analysis of the GNPTAB and GNPTG genes in 13 patients with mucolipidosis type II or type III - identification of eight novel mutations. *Clin. Genet.* **76,** 76–84
18. Gao, Y., Yang, K., Xu, S., Wang, C., Liu, J., Zhang, Z., Yuan, M., Luo, X., Liu, M., Wang, Q. K., and Liu, J. Y. (2011) Identification of compound heterozygous mutations in GNPTG in three siblings of a Chinese family with mucolipidosis type III gamma. *Mol. Genet. Metab.* **102,** 107–109
19. Liu, S., Zhang, W., Shi, H., Meng, Y., and Qiu, Z. (2014) Three novel homozygous mutations in the GNPTG gene that cause mucolipidosis type III gamma. *Gene* **535,** 294–298
20. Persichetti, E., Chuzhanova, N. A., Dardis, A., Tappino, B., Pohl, S., Thomas, N. S., Rosano, C., Balducci, C., Paciotti, S., Dominissini, S., Montalvo, A. L., Sibilio, M., Parini, R., Rigoldi, M., Di Rocco, M., Parenti, G., Orlacchio, A., Bembi, B., Cooper, D. N., Filocamo, M., and Beccari, T. (2009) Identification and molecular characterization of six novel mutations in the UDP-N-acetylglucosamine-1-phosphotransferase gamma subunit (GNPTG) gene in patients with mucolipidosis III gamma. *Hum. Mutat.* **30,** 978–984
21. Pohl, S., Encarnação, M., Castrichini, M., Müller-Loennies, S., Muschol, N., and Braulke, T. (2010) Loss of N-Acetylglucosamine-1-phosphotransferase gamma-subunit due to intronic mutation in GNPTG causes mucolipidosis type III gamma: Implications for molecular and cellular diagnostics. *Am. J. Med. Genet. A.* **152A,** 124–132
22. Raas-Rothschild, A., Bargal, R., Goldman, O., Ben-Asher, E., Groener, J. E., Toutain, A., Stemmer, E., Ben-Neriah, Z., Flusser, H., Beemer, F. A., Penttinen, M., Olender, T., Rein, A. J., Bach, G., and Zeigler, M. (2004) Genomic organisation of the UDP-N-acetylglucosamine-1-phosphotransferase gamma subunit (GNPTAG) and its mutations in mucolipidosis III. *J. Med. Genet.* **41,** e52
23. Schrader, K. A., Heravi-Moussavi, A., Waters, P. J., Senz, J., Whelan, J., Ha, G., Eydoux, P., Nielsen, T., Gallagher, B., Oloumi, A., Boyd, N., Fernandez, B. A., Young, T. L., Jones, S. J., Hirst, M., Shah, S. P., Marra, M. A., Green, J., and Huntsman, D. G. (2011) Using next-generation sequencing for the diagnosis of rare disorders: a family with retinitis pigmentosa and skeletal abnormalities. *J. Pathol.* **225,** 12–18
24. Tiede, S., Cantz, M., Raas-Rothschild, A., Muschol, N., Bürger, F., Ullrich, K., and Braulke, T. (2004) A novel mutation in UDP-N-acetylglucosamine-1-phosphotransferase gamma subunit (GNPTAG) in two siblings with mucolipidosis type III alters a used glycosylation site. *Hum. Mutat.* **24,** 535
25. Tüysüz, B., Kasapcopur, O., Alkaya, D. U., Sahin, S., Sozeri, B., and Yesil, G. (2018) Mucolipidosis type III gamma: Three novel mutation and genotype-phenotype study in eleven patients. *Gene* **642,** 398–407
26. Velho, R. V., Alegra, T., Sperb, F., Ludwig, N. F., Saraiva-Pereira, M. L., Matte, U., and Schwartz, I. V. (2014) A de novo or germline mutation in a family with Mucolipidosis III gamma: Implications for molecular diagnosis and genetic counseling. *Mol. Genet. Metab. Rep.* **1,** 98–102
27. Velho, R. V., Ludwig, N. F., Alegra, T., Sperb-Ludwig, F., Guarany, N. R., Matte, U., and Schwartz, I. V. (2016) Enigmatic in vivo GlcNAc-1-phosphotransferase (GNPTG) transcript correction to wild type in two mucolipidosis III gamma siblings homozygous for nonsense mutations. *J. Hum. Genet.* **61,** 555–560
28. Zrhidri, A., Amasdl, S., Lyahyai, J., Elouardi, H., Chkirate, B., Raymond, L., Egea, G., Taoudi, M., El Mouatassim, S., and Sefiani, A. (2017) Next Generation Sequencing identifies mutations in GNPTG gene as a cause of familial form of scleroderma-like disease. *Pediatr Rheumatol. Online J.* **15,** 72
29. Kollmann, K., Pohl, S., Marschner, K., Encarnação, M., Sakwa, I., Tiede, S., Poorthuis, B. J., Lübke, T., Müller-Loennies, S., Storch, S., and Braulke, T. (2010) Mannose phosphorylation in health and disease. Eur. J. *Cell. Biol.* **89,** 117–123
30. Raas-Rothschild, A., Pohl, S., and Braulke, T., *Multiple enzyme deficiencies: Defects in transport: Mucolipidosis II alpha/beta; mucolipidosis III alpha/beta and mucolipidosis III gamma*, in *Lysosomal storage diseases: A practical guide*, A.B. Mehta and B. Winchester, Editors. 2012, WILEY-BLACKWELL: Oxford. p. 121–126
31. Kelly, T. E., Thomas, G. H., Taylor, H. A., Jr, McKusick, V. A., Sly, W. S., Glaser, J. H., Robinow, M., Luzzatti, L., Espiritu, C., Feingold, M., Bull, M. J., Ashenhurst, E. M., and Ives, E. J. (1975) Mucolipidosis III (pseudo-Hurler polydystrophy): Clinical and laboratory studies in a series of 12 patients. *Johns Hopkins Med. J.* **137,** 156–175
32. Smuts, I., Potgieter, D., and van der Westhuizen, F. H. (2009) Combined tarsal and carpal tunnel syndrome in mucolipidosis type III. A case study and review. *Ann. N.Y. Acad. Sci.* **1151,** 77–84
33. Umehara, F., Matsumoto, W., Kuriyama, M., Sukegawa, K., Gasa, S., and Osame, M. (1997) Mucolipidosis III (pseudo-Hurler polydystrophy); clinical studies in aged patients in one family. *J. Neurol. Sci.* **146,** 167–172
34. Köhne, T., Markmann, S., Schweizer, M., Muschol, N., Friedrich, R. E., Hagel, C., Glatzel, M., Kahl-Nieke, B., Amling, M., Schinke, T., and Braulke, T. (2016) Mannose 6-phosphate-dependent targeting of lysosomal enzymes is required for normal craniofacial and dental development. *Biochim. Biophys. Acta* **1862,** 1570–1580
35. Otomo, T., Schweizer, M., Kollmann, K., Schumacher, V., Muschol, N., Tolosa, E., Mittrucker, H. W., and Braulke, T. (2015) Mannose 6 phosphorylation of lysosomal enzymes controls B cell functions. *J. Cell Biol.* **208,** 171–180
36. Owada, M., and Neufeld, E. F. (1982) Is there a mechanism for introducing acid hydrolases into liver lysosomes that is independent of mannose 6-phosphate recognition? Evidence from I-cell disease. *Biochem. Biophys. Res. Commun.* **105,** 814–820
37. Waheed, A., Pohlmann, R., Hasilik, A., von Figura, K., van Elsen, A., and Leroy, J. G. (1982) Deficiency of UDP-N-acetylglucosamine:lysosomal enzyme N-acetylglucosamine-1-phosphotransferase in organs of I-cell patients. *Biochem. Biophys. Res. Commun.* **105,** 1052–1058
38. Markmann, S., Thelen, M., Cornils, K., Schweizer, M., Brocke-Ahmadinejad, N., Willnow, T., Heeren, J., Gieselmann, V., Braulke, T., and Kollmann, K. (2015) Lrp1/LDL receptor play critical roles in mannose 6-phosphate-independent lysosomal enzyme targeting. *Traffic* **16,** 743–759
39. Harmatz, P., and Shediac, R. (2017) Mucopolysaccharidosis VI: pathophysiology, diagnosis and treatment. *Front. Biosci.* **22,** 385–406
40. De Pace, R., Coutinho, M. F., Koch-Nolte, F., Haag, F., Prata, M. J., Alves, S., Braulke, T., and Pohl, S. (2014) Mucolipidosis II-related mutations inhibit the exit from the endoplasmic reticulum and proteolytic cleavage of GlcNAc-1-phosphotransferase precursor protein GNPTAB. *Hum. Mutat.* **35,** 368–376
41. Müller-Loennies, S., Galliciotti, G., Kollmann, K., Glatzel, M., and Braulke, T. (2010) A novel single chain antibody fragment for detection of mannose 6-phosphate-containing proteins: Application in mucolipidosis type II patients and mice. *Am. J. Pathol.* **177,** 240–247
42. Zachos, C., Blanz, J., Saftig, P., and Schwake, M. (2012) A critical histidine residue within LIMP-2 mediates pH sensitive binding to its ligand beta-glucocerebrosidase. *Traffic* **13,** 1113–1123
43. Deuschl, F., Kollmann, K., von Figura, K., and Lubke, T. (2006) Molecular characterization of the hypothetical 66.3-kDa protein in mouse: lysosomal targeting, glycosylation, processing and tissue distribution. *FEBS Lett.* **580,** 5747–5752
44. Kornak, U., Kasper, D., Bosl, M. R., Kaiser, E., Schweizer, M., Schulz, A., Friedrich, W., Delling, G., and Jentsch, T. J. (2001) Loss of the ClC-7 chloride channel leads to osteopetrosis in mice and man. *Cell* **104,** 205–215

45. Rodriguez, C. I., Buchholz, F., Galloway, J., Sequerra, R., Kasper, J., Ayala, R., Stewart, A. F., and Dymecki, S. M. (2000) High-efficiency deleter mice show that FLPe is an alternative to Cre-loxP. *Nat. Genet.* **25,** 139–140
46. Schwenk, F., Baron, U., and Rajewsky, K. (1995) A cre-transgenic mouse strain for the ubiquitous deletion of loxP-flanked gene segments including deletion in germ cells. *Nucleic Acids Res.* **23,** 5080–5081
47. Weber, K., Bartsch, U., Stocking, C., and Fehse, B. (2008) A multicolor panel of novel lentiviral "gene ontology" (LeGO) vectors for functional gene analysis. *Mol. Ther.* **16,** 698–706
48. Suter, A., Everts, V., Boyde, A., Jones, S. J., Lüllmann-Rauch, R., Hartmann, D., Hayman, A. R., Cox, T. M., Evans, M. J., Meister, T., von Figura, K., and Saftig, P. (2001) Overlapping functions of lysosomal acid phosphatase (LAP) and tartrate-resistant acid phosphatase (Acp5) revealed by doubly deficient mice. *Development* **128,** 4899–4910
49. Lawrence, R., Brown, J. R., Al-Mafraji, K., Lamanna, W. C., Beitel, J. R., Boons, G. J., Esko, J. D., and Crawford, B. E. (2012) Disease-specific non-reducing end carbohydrate biomarkers for mucopolysaccharidoses. *Nat. Chem. Biol.* **8,** 197–204
50. Lamanna, W. C., Lawrence, R., Sarrazin, S., and Esko, J. D. (2011) Secondary storage of dermatan sulfate in Sanfilippo disease. *J. Biol. Chem.* **286,** 6955–6962
51. Kollmann, K., Damme, M., Markmann, S., Morelle, W., Schweizer, M., Hermans-Borgmeyer, I., Röchert, A. K., Pohl, S., Lübke, T., Michalski, J. C., Kakela, R., Walkley, S. U., and Braulke, T. (2012) Lysosomal dysfunction causes neurodegeneration in mucolipidosis II 'knock-in' mice. *Brain* **135,** 2661–2675
52. Velho, R. V., De Pace, R., Klünder, S., Sperb-Ludwig, F., Lourenco, C. M., Schwartz, I. V., Braulke, T., and Pohl, S. (2015) Analyses of disease-related GNPTAB mutations define a novel GlcNAc-1-phosphotransferase interaction domain and an alternative site-1 protease cleavage site. *Hum. Mol. Genet.* **24,** 3497–3505
53. Thelen, M., Winter, D., Braulke, T., and Gieselmann, V. (2017) SILAC-based comparative proteomic analysis of lysosomes from mammalian cells using LC-MS/MS. *Methods Mol. Biol.* **1594,** 1–18
54. Rappsilber, J., Mann, M., and Ishihama, Y. (2007) Protocol for micro-purification, enrichment, pre-fractionation and storage of peptides for proteomics using StageTips. *Nat. Protoc.* **2,** 1896–1906
55. Hahne, H., Pachl, F., Ruprecht, B., Maier, S. K., Klaeger, S., Helm, D., Medard, G., Wilm, M., Lemeer, S., and Kuster, B. (2013) DMSO enhances electrospray response, boosting sensitivity of proteomic experiments. *Nat. Methods* **10,** 989–991
56. Ritchie, M. E., Phipson, B., Wu, D., Hu, Y., Law, C. W., Shi, W., and Smyth, G. K. (2015) limma powers differential expression analyses for RNA-sequencing and microarray studies. *Nucleic Acids Res.* **43,** e47
57. Schwämmle, V., Leon, I. R., and Jensen, O. N. (2013) Assessment and improvement of statistical tools for comparative proteomics analysis of sparse data sets with few experimental replicates. *J. Proteome Res.* **12,** 3874–3883
58. Storey, J. D. (2002) A direct approach to false discovery rates. *R. Stat. Soc. Series B Stat. Methodol.* **64,** 479–498
59. Cox, J., and Mann, M. (2008) MaxQuant enables high peptide identification rates, individualized p.p.b.-range mass accuracies and proteome-wide protein quantification. *Nat. Biotechnol.* **26,** 1367–1372
60. DeBose-Boyd, R. A., Brown, M. S., Li, W. P., Nohturfft, A., Goldstein, J. L., and Espenshade, P. J. (1999) Transport-dependent proteolysis of SREBP: relocation of site-1 protease from Golgi to ER obviates the need for SREBP transport to Golgi. *Cell* **99,** 703–712
61. Reczek, D., Schwake, M., Schröder, J., Hughes, H., Blanz, J., Jin, X., Brondyk, W., Van Patten, S., Edmunds, T., and Saftig, P. (2007) LIMP-2 is a receptor for lysosomal mannose-6-phosphate-independent targeting of beta-glucocerebrosidase. *Cell* **131,** 770–783
62. Braulke, T., Geuze, H. J., Slot, J. W., Hasilik, A., and von Figura, K. (1987) On the effects of weak bases and monensin on sorting and processing of lysosomal enzymes in human cells. *Eur. J. Cell Biol.* **43,** 316–321
63. Ohkuma, S., and Poole, B. (1978) Fluorescence probe measurement of the intralysosomal pH in living cells and the perturbation of pH by various agents. *Proc. Natl. Acad. Sci. U.S.A.* **75,** 3327–3331
64. Braulke, T., Gartung, C., Hasilik, A., and von Figura, K. (1987) Is movement of mannose 6-phosphate-specific receptor triggered by binding of lysosomal enzymes? *J. Cell Biol.* **104,** 1735–1742
65. Vogel, P., Payne, B. J., Read, R., Lee, W. S., Gelfman, C. M., and Kornfeld, S. (2009) Comparative Pathology of Murine Mucolipidosis Types II and IIIC. *Vet. Pathol.* **46,** 313–324
66. Flanagan-Steet, H., Matheny, C., Petrey, A., Parker, J., and Steet, R. (2016) Enzyme-specific differences in mannose phosphorylation between GlcNAc-1-phosphotransferase alphabeta and gamma subunit deficient zebrafish support cathepsin proteases as early mediators of mucolipidosis pathology. *Biochim. Biophys. Acta* **1860,** 1845–1853
67. Wang, M. L., Motamed, M., Infante, R. E., Abi-Mosleh, L., Kwon, H. J., Brown, M. S., and Goldstein, J. L. (2010) Identification of surface residues on Niemann-Pick C2 essential for hydrophobic handoff of cholesterol to NPC1 in lysosomes. *Cell Metab.* **12,** 166–173
68. Hait, N. C., Allegood, J., Maceyka, M., Strub, G. M., Harikumar, K. B., Singh, S. K., Luo, C., Marmorstein, R., Kordula, T., Milstien, S., and Spiegel, S. (2009) Regulation of histone acetylation in the nucleus by sphingosine-1-phosphate. *Science* **325,** 1254–1257
69. Pipalia, N. H., Cosner, C. C., Huang, A., Chatterjee, A., Bourbon, P., Farley, N., Helquist, P., Wiest, O., and Maxfield, F. R. (2011) Histone deacetylase inhibitor treatment dramatically reduces cholesterol accumulation in Niemann-Pick type C1 mutant human fibroblasts. *Proc. Natl. Acad. Sci. U.S.A.* **108,** 5620–5625
70. Newton, J., Hait, N. C., Maceyka, M., Colaco, A., Maczis, M., Wassif, C. A., Cougnoux, A., Porter, F. D., Milstien, S., Platt, N., Platt, F. M., and Spiegel, S. (2017) FTY720/fingolimod increases NPC1 and NPC2 expression and reduces cholesterol and sphingolipid accumulation in Niemann-Pick type C mutant fibroblasts. *FASEB J.* **31,** 1719–1730
71. Markmann, S., Krambeck, S., Hughes, C. J., Mirzaian, M., Aerts, J. M., Saftig, P., Schweizer, M., Vissers, J. P., Braulke, T., and Damme, M. (2017) Quantitative proteome analysis of mouse liver lysosomes provides evidence for mannose 6-phosphate-independent targeting mechanisms of acid hydrolases in mucolipidosis II. *Mol. Cell. Proteomics* **16,** 438–450
72. Baker, P. R., and Chalkley, R. J. (2014) MS-viewer: a web-based spectral viewer for proeomics results. *Mol. Cell. Proteomics* **13,** 1392–1396